ELSEVIER

Journal of Volcanology and Geothermal Research 108 (2001) 303–341

Journal of volcanology and geothermal research

www.elsevier.com/locate/jvolgeores

Magmatic gas scrubbing: implications for volcano monitoring

R.B. Symonds[a,*], T.M. Gerlach[a], M.H. Reed[b]

[a]*U.S. Geological Survey, Cascades Volcano Observatory, 5400 MacArthur Blvd., Vancouver, WA 98661, USA*
[b]*Department of Geological Sciences, University of Oregon, Eugene, OR 97403, USA*

Abstract

Despite the abundance of $SO_{2(g)}$ in magmatic gases, precursory increases in magmatic $SO_{2(g)}$ are not always observed prior to volcanic eruption, probably because many terrestrial volcanoes contain abundant groundwater or surface water that scrubs magmatic gases until a dry pathway to the atmosphere is established. To better understand scrubbing and its implications for volcano monitoring, we model thermochemically the reaction of magmatic gases with water. First, we inject a 915°C magmatic gas from Merapi volcano into 25°C air-saturated water (ASW) over a wide range of gas/water mass ratios from 0.0002 to 100 and at a total pressure of 0.1 MPa. Then we model closed-system cooling of the magmatic gas, magmatic gas-ASW mixing at 5.0 MPa, runs with varied temperature and composition of the ASW, a case with a wide range of magmatic–gas compositions, and a reaction of a magmatic gas–ASW mixture with rock. The modeling predicts gas and water compositions, and, in one case, alteration assemblages for a wide range of scrubbing conditions; these results can be compared directly with samples from degassing volcanoes. The modeling suggests that $CO_{2(g)}$ is the main species to monitor when scrubbing exists; another candidate is $H_2S_{(g)}$, but it can be affected by reactions with aqueous ferrous iron. In contrast, scrubbing by water will prevent significant $SO_{2(g)}$ and most $HCl_{(g)}$ emissions until dry pathways are established, except for moderate $HCl_{(g)}$ degassing from $pH < 0.5$ hydrothermal waters. Furthermore, it appears that scrubbing will prevent much, if any, $SO_{2(g)}$ degassing from long-resident boiling hydrothermal systems. Several processes can also decrease or increase $H_{2(g)}$ emissions during scrubbing making $H_{2(g)}$ a poor choice to detect changes in magma degassing.

We applied the model results to interpret field observations and emission rate data from four eruptions: (1) Crater Peak on Mount Spurr (1992) where, except for a short post-eruptive period, scrubbing appears to have drastically diminished pre-, inter-, and post-eruptive $SO_{2(g)}$ emissions, but had much less impact on $CO_{2(g)}$ emissions. (2) Mount St. Helens where scrubbing of $SO_{2(g)}$ was important prior to and three weeks after the 18 May 1980 eruption. Scrubbing was also active during a period of unrest in the summer of 1998. (3) Mount Pinatubo where early drying out prevented $SO_{2(g)}$ scrubbing before the climactic 15 June 1991 eruption. (4) The ongoing eruption at Popocatépetl in an arid region of Mexico where there is little evidence of scrubbing.

In most eruptive cycles, the impact of scrubbing will be greater during pre- and post-eruptive periods than during the main eruptive and intense passive degassing stages. Therefore, we recommend monitoring the following gases: $CO_{2(g)}$ and $H_2S_{(g)}$ in precursory stages; $CO_{2(g)}$, $H_2S_{(g)}$, $SO_{2(g)}$, $HCl_{(g)}$, and $HF_{(g)}$ in eruptive and intense passive degassing stages; and $CO_{2(g)}$ and $H_2S_{(g)}$ again in the declining stages. $CO_{2(g)}$ is clearly the main candidate for early emission rate monitoring, although significant early increases in the intensity and geographic distribution of $H_2S_{(g)}$ emissions should be taken as an important sign of volcanic unrest and a potential precursor. Owing to the difficulty of extracting $SO_{2(g)}$ from hydrothermal waters, the emergence of >100 t/d (tons per day) of $SO_{2(g)}$ in addition to $CO_{2(g)}$ and $H_2S_{(g)}$ should be taken as a criterion of magma intrusion. Finally, the modeling suggests that the interpretation of gas-ratio data requires a case-by-case evaluation since ratio changes can often be produced by several mechanisms; nevertheless, several gas ratios may provide useful indices for monitoring the drying out of gas pathways. Published by Elsevier Science B.V.

Keywords: scrubbing; volcanic emissions; volcanic gases; degassing; monitoring; hydrothermal system; volcano

* Corresponding author. Present address: Drilling Company, Ground-Water Research Program, PO Box 15287, Al Ain, Abu Dhabi Emirate, United Arab Emirates. Tel.: +971-3-7612544.

E-mail address: bsymonds@usgs.gov (R.B. Symonds).

0377-0273/01/$ - see front matter. Published by Elsevier Science B.V.
PII: S0377-0273(00)00292-4

1. Introduction

Along with seismic and geodetic monitoring, gas studies play an important role in monitoring potentially restless volcanoes. The main purpose for monitoring gases from a re-awakening volcano is to help detect the intrusion of magma. The dominant magmatic gases are $H_2O_{(g)}$, $CO_{2(g)}$, and $SO_{2(g)}$ followed by smaller concentrations of $H_{2(g)}$, $H_2S_{(g)}$, $HCl_{(g)}$, $HF_{(g)}$, $CO_{(g)}$, $S_{2(g)}$, $COS_{(g)}$, and rare gases (Symonds et al., 1994). Increased emissions (or concentrations) of $CO_{2(g)}$ and $SO_{2(g)}$ are the obvious gas precursors of magmatic intrusion in part because $H_2O_{(g)}$ may derive from magmatic or meteoric sources. Over the past two decades, gas monitoring has relied heavily on measuring $SO_{2(g)}$ emission rates because it can be determined easily with the ultraviolet-sensing correlation spectrometer (COSPEC).

Some eruptions are preceded by the expected large increase in $SO_{2(g)}$ emission rates as was the situation prior to the 1991 eruptions of Mount Pinatubo (Daag et al., 1996). In contrast, before and after the 1992 eruptions of Mount Spurr, there were generally very low emission rates of $SO_{2(g)}$ despite the high emission rates of $SO_{2(g)}$ during eruptions and persistently elevated seismic activity (Doukas and Gerlach, 1995). Doukas and Gerlach (1995) also observed elevated $CO_{2(g)}$ emissions and significant $H_2S_{(g)}$ odor in the plume during the repose periods between eruptions. They argue that water within the volcanic edifice interacted with rising magmatic gases; this water reduced $SO_{2(g)}$ emissions by hydrolysis or scrubbing reactions, but had much less impact on less-water-soluble gases like $CO_{2(g)}$ and $H_2S_{(g)}$. Here we define scrubbing more broadly than Doukas and Gerlach (1995) to encompass any process that reduces emissions during reactions between magmatic gas, water, and sometimes rock; hence, scrubbing includes dissolution into the aqueous phase (e.g. hydrolysis) and formation of precipitates (e.g. sulfur, sulfides, fluorides, and sulfates) from gas–water or gas–water–rock reactions.

In this study, we use thermochemical modeling to evaluate scrubbing of magmatic gases by groundwaters and surface waters of volcanoes (hereafter, volcano waters). The models permit quantitative investigation of the details of scrubbing over a wide range of conditions. We constrain the calculations with analyses of high-temperature magmatic gases to assure that the scenarios we examine are realistic. The main intent of the work is to show which gases are promising candidates for monitoring at various stages in a cycle of volcanic unrest from early precursory stages to post-eruption.

Investigators of hydrothermal systems and ore deposits have long embraced the idea that hydrothermal fluids absorb volatiles degassed from shallow magma (White, 1957; Hemley and Jones, 1964; Burnham, 1979; Brimhall and Ghiorso, 1983; Giggenbach, 1988; Hedenquist and Lowenstern, 1994; Reed, 1997). These studies indicate that magma-derived sulfur, halogen gases, and carbon dioxide acidify hydrothermal systems and promote alteration and mineralization. Direct injection of magmatic gases into meteoric groundwater or volcanic crater lakes produces acidic hydrothermal fluids. Magmatic gases can also generate acidic hydrothermal fluids in situ when they condense upon cooling, forming a water-rich liquid that absorbs coexisting acid gases, and which may subsequently mix with meteoric water (Rye et al., 1992; Rye, 1993). In early thermochemical modeling of hydrothermal systems, Holland (1965) demonstrated that essentially all magmatic $SO_{2(g)}$ is consumed by hydrolysis reactions involving disproportionations:

$$4SO_{2(g)} + 4H_2O_{(aq)} = H_2S_{(aq)} + 3H_2SO_{4(aq)}, \quad (1)$$

and

$$3SO_{2(g)} + 2H_2O_{(aq)} = S_{(s,l)} + 2H_2SO_{4(aq)}. \quad (2)$$

These reactions shift strongly to the right with cooling below 400°C. Reaction with iron to form pyrite or other Fe sulfides may remove much of the $H_2S_{(g)}$ produced by $SO_{2(g)}$ hydrolysis (Rye, 1993). Experimental studies and thermochemical modeling of volatile partitioning between vapor and liquid in moderate temperature (100–350°C), two-phase hydrothermal systems show that after $CO_{2(g)}$, $H_2S_{(g)}$ is the most abundant hydrothermal gas and that other sulfurous gases (e.g. $SO_{2(g)}$ and $S_{2(g)}$) are negligible (Drummond and Ohmoto, 1985; Giggenbach, 1980; Reed and Spycher, 1984, 1985; Spycher and Reed, 1989). According to thermodynamic models (Gerlach et al., 1996), even flash-vaporization (e.g. rapid and complete boiling) of sulfate-rich hydrothermal fluid at 400–800°C fails to liberate significant amounts of

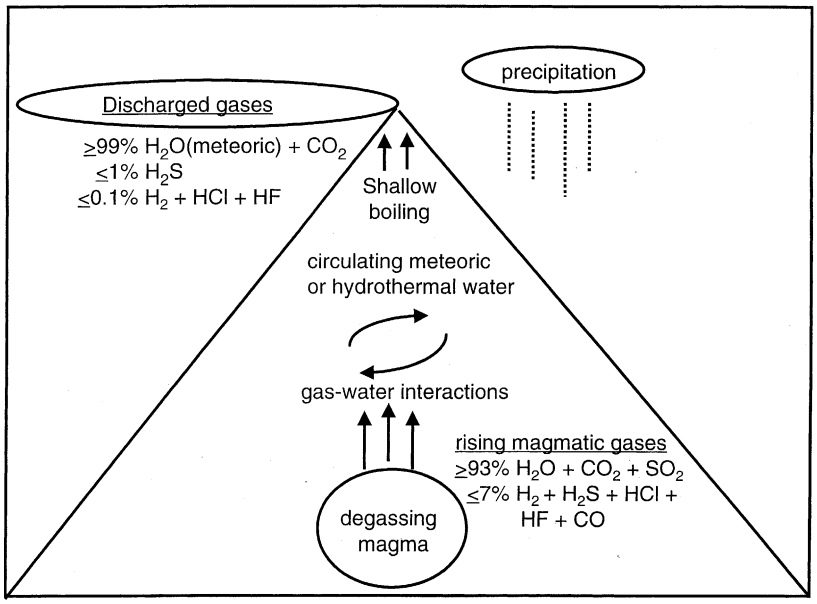

Fig. 1. Diagram of a hypothetical degassing volcano where rising gases from degassing magma are scrubbed by meteoric or hydrothermal water in the volcanic edifice. Scrubbing processes including hydrolysis, precipitation, and water–rock reaction modify the magmatic gases to produce gas emissions dominated by $H_2O_{(g)}$, $CO_{2(g)}$, and $H_2S_{(g)}$.

$SO_{2(g)}$; instead, nearly all dissolved sulfate precipitates as sulfate minerals. Thus, once magmatic $SO_{2(g)}$ is scrubbed, sulfur is unlikely to be degassed again as $SO_{2(g)}$ from a boiling hydrothermal system.

Observations on present-day magmatic hydrothermal systems in volcanic settings support the hypothesis that magmatic gases acidify hydrothermal fluids and confirm that $SO_{2(g)}$ hydrolysis is widespread (Henley and Ellis, 1983; Kiyosu and Kurahashi, 1983; Giggenbach, 1987; Sturchio et al., 1988; Williams et al., 1990). Well fluids provide a dramatic example of $SO_{2(g)}$ hydrolysis at the Krafla geothermal field (Armannsson et al., 1982) where the scrubbing of $SO_{2(g)}$ in magmatic gases emanating from a magma chamber under the field can be traced during passage through the hydrothermal system; in this case, $SO_{2(g)}$ hydrolysis forms highly mobile $H_2S_{(g)}$, although formation of iron sulfide removes substantial amounts of the $H_2S_{(g)}$ by reaction with $Fe^{2+}_{(aq)}$ dissolved from basaltic glass, magnetite, and pyroxene. Several studies of volcanic crater lakes provide especially vivid examples of the acidifying influence of magmatic volatiles on hydrothermal systems and the control exerted by $SO_{2(g)}$ disproportionation on sulfur precipitation and dissolved sulfate, polythionate, and sulfide species (Casadevall et al., 1984; Takano and Watanuki, 1990; Rowe et al., 1992; Pasternack and Varekamp, 1994; Rowe, 1994; Takano et al., 1994). Samples of subseafloor hydrothermal vents also reveal magmatic volatiles in the vent fluids, notably magmatic $CO_{2(g)}$ and sulfate from hydrolysis of magmatic $SO_{2(g)}$ (Sedwick et al., 1992).

2. Numerical modeling

2.1. Working hypothesis; initial and boundary conditions

We model scrubbing for an inactive volcano that has just been intruded by magma (Fig. 1), although scrubbing can occur during any stage of the eruptive cycle. The edifice or degassing pathway(s) contain(s) sufficient water to scrub exsolved volatiles from the newly intruded magma. Note that venting of unscrubbed magmatic volatiles from magma to atmosphere may only require drying of a narrow dry crack rather than depleting water from the entire edifice. In

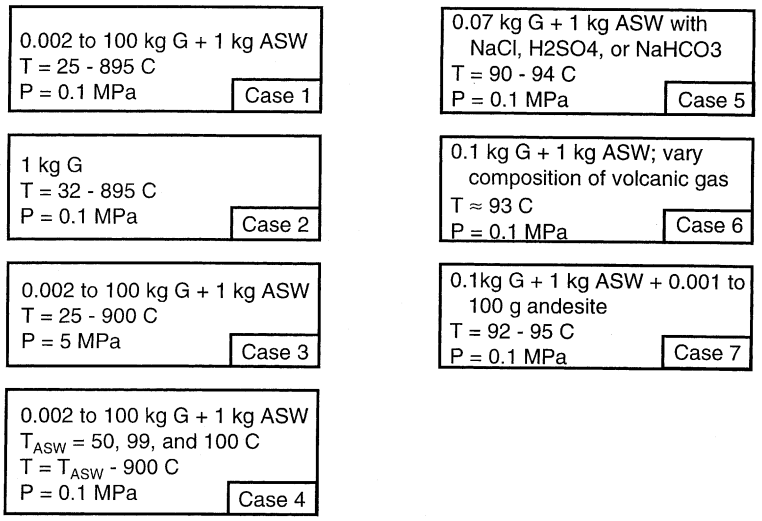

Fig. 2. Diagram showing the magmatic gas–water mixing processes simulated in this study. G and ASW refer to the 915°C Merapi gas (Table 1) and ASW, respectively. In case 1, we inject variable amounts of the Merapi gas into 1 kg of 25°C ASW at 0.1 MPa. Case 2 is closed-system cooling of the Merapi gas. Case 3 explores the effects of using 5 MPa pressure on the case 1 calculations. Case 4 repeats the case 1 calculations using 50°, 99°, and 100°C ASW. In case 5, we add variable amounts of $H_2SO_{4(s)}$, $NaCl_{(s)}$, and $NaHCO_{3(s)}$ to the starting ASW. In case 6, we vary the magmatic gas composition from Merapi 79-2. In case 7, we add variable amounts of andesite to a Merapi gas–ASW mixture.

our hypothetical scenario, the newly intruded magma begins discharging heat and magmatic gases into the volcanic edifice. Rising magmatic gases containing ≥93% $H_2O_{(g)} + CO_{2(g)} + SO_{2(g)}$ and ≤7% $H_{2(g)} + H_2S_{(g)} + HCl_{(g)} + HF_{(g)} + CO_{(g)}$ (e.g. Symonds et al., 1994) react with circulating waters, which may be dilute waters from direct precipitation or melting of snow and ice, or more saline hydrothermal waters. The amount of water that reacts with gas, expressed as the gas/water (g/w) ratio, depends on the amount of injected heat and gas from the magma, and the porosity, permeability, and amount of water stored in the edifice. Another factor is reaction of the mixture with rock. Scrubbed volcanic-gas discharges consist either of cold $CO_{2(g)}$-rich emissions or heated emissions containing ≥99% $H_2O_{(g)} + CO_{2(g)}$, ≤1% $H_2S_{(g)}$, and ≤0.1% $N_{2(g)} + H_{2(g)} + HCl_{(g)} + HF_{(g)}$ based on gas compositions from low-temperature volcanic fumaroles (Symonds et al., 2001), Scrubbing Case Studies (Section 3), and numerical modeling results (Sections 2.4–2.11).

The main variables in the magmatic gas–water mixing reaction are the initial compositions and temperatures of the water and the magmatic gas, the confining pressure, the g/w ratio, and the extent of reaction between the gas–water mixture and rock. The predominant volcano waters are: (1) dilute meteoric waters (essentially air-saturated water; hereafter ASW); (2) acid-sulfate waters with pH = 0–4 and up to 100,000 ppm $SO^{2-}_{4(aq)}$; (3) neutral chloride waters with up to 100,000 ppm $Cl^{-}_{(aq)}$ balanced by $Na^{+}_{(aq)}$ or $Ca^{2+}_{(aq)}$; and (4) bicarbonate waters that are slightly acidic (pH 4–7) and, at higher pressures, contain up to 100,000 ppm $HCO^{-}_{3(aq)}$ mostly balanced by $Na^{+}_{(aq)}$, $Ca^{2+}_{(aq)}$, and $H^{+}_{(aq)}$ (White, 1957; Ellis and Mahon, 1977; Giggenbach et al., 1990). The temperatures of these waters range from ~20°C to their boiling points at the confining pressure. The compositions of high-temperature magmatic gases range widely: 30–99.9% $H_2O_{(g)}$, 0.01–55% $CO_{2(g)}$, 0.005–50% $SO_{2(g)}$, 0.01–3% $H_{2(g)}$, 0.004–3% $H_2S_{(g)}$, 0.02–1% $HCl_{(g)}$, and 0.01–0.2% $HF_{(g)}$ (Symonds et al., 1994, excluding high halogen concentrations from Augustine and Momotombo). The temperatures of the source magmas for volcanic gases are typically 900–1200°C. The pressure around degassing magma bodies ranges from 0.1 to several hundred megaPascal; for purposes of this paper we restrict our investigation to the pressures of 0.1–5 MPa (1–50 bar). The g/w ratios in degassing volcanoes

Table 1
Composition of the Merapi gas analysis used for modeling in this paper. The data is for sample 79-2 from Le Guern et al. (1982). All data in mol% (T_{vent} is the vent temperature and T_{eq} is the equilibrium temperature of the composition)

Species	Concentration
H_2O	88.87
CO_2	7.07
H_2	1.54
SO_2	1.15
H_2S	1.12
HCl	0.59
CO	0.16
S_2	0.08
HF	0.04
T_{vent} (°C)	810
T_{eq} (°C)	915

obviously ranges from zero (entirely water) to infinity (pure magmatic gas).

2.2. Outline, assumptions, and limitations of modeling

Using the above constraints, we investigate the scrubbing process by modeling seven cases (Fig. 2). In case 1, we inject increments of hot magmatic gas into 1 kg of 25°C ASW (with 4.5×10^{-4} mol $N_{2(aq)}$ and 2.4×10^{-4} mol $O_{2(aq)}$) at 0.1 MPa to study near-surface scrubbing. The magmatic gas is sample 79-2 from Merapi Volcano, Indonesia (Table 1; Le Guern et al., 1982), which we selected because it is representative of high-temperature convergent-plate volcanic gases, and its 915°C equilibrium temperature suggests a large magmatic component (Symonds et al., 1994). Note that air components ($N_{2(g)}$, $O_{2(g)}$, Ar) were removed from the 79-2 analysis by Le Guern et al. (1982) when retrieving the equilibrium composition. ASW was chosen because most ≤300°C volcano waters are meteoric in origin and this dilute solution provides a simple baseline for the study of gas–water reactions.

We compare the results from case 1 to simple closed-system cooling of the Merapi gas (case 2) in which we examine the scrubbing effects of in situ condensate formation. Case 3 involves the same process as case 1, but at the higher pressure of 5 MPa, to study subsurface scrubbing. Case 4 involves mixing of the Merapi gas with 50, 99, and 100°C ASW to study the effect of ASW preheating by conduction. In case 5, we add incremental amounts of $H_2SO_{4(s)}$, $NaCl_{(s)}$,or $NaHCO_{3(s)}$ to three separate batches of starting ASW to simulate the effect of injecting magmatic gas into acid sulfate, neutral chloride, and bicarbonate waters, respectively. In case 6, we vary the composition of the magmatic gas from Merapi 79-2, one species at a time, to cover the natural range of gases from volcanic magmas. In case 7, we add variable amounts of andesite to a magmatic gas–ASW mixture to study the effect of rock reaction on the calculations.

The modeling is necessarily a simplification of the natural process, most notably in that scrubbing in degassing volcanoes is probably not entirely an equilibrium process. In particular, reaction kinetics and the dynamic flow rate of magmatic gas from depth may influence the extent of gas–water reaction and, therefore, the compositions of gas discharges. Nonetheless, by varying the main input parameters in multiple calculations and comparing the results to observations at degassing volcanoes, it is possible to acquire understanding of the natural process.

2.3. Numerical methods

The modeling involves computing chemical equilibria in mixtures of high-temperature magmatic gases, volcano waters, and, in one instance, volcanic rock over a range of temperature, pressure, and compositional conditions. The computed mixtures range from pure liquid to liquid-plus-gas to pure gas. To model this wide spectrum of mixtures, it is necessary to use two chemical-equilibria computer programs. We use program CHILLER (Reed, 1982, 1998; Spycher and Reed, 1988) to model the pure-liquid and liquid-plus-gas regions of the calculations whereas we employ program GASWORKS (Symonds and Reed, 1993) to model the pure-gas region. CHILLER calculates heterogeneous chemical equilibria in aqueous–gas–solid systems during processes of heating (or cooling), fluid–fluid mixing, boiling (or condensing), water–rock reaction, evaporation, and oxidation. The program solves a series of mass-balance, mass-action, and, for selected boiling calculations, enthalpy-balance equations. The enthalpy balance constraint enables computation of high degrees of boiling (>90 wt% gas). CHILLER also has the capability of

Table 2
Aqueous, gas, mineral, and liquid species used in the thermochemical modeling in this paper

Aqueous species[a]							
CO_3^{2-}	HCl	HSO_5^-	NO_2^-	$NaHCO_3$	SO_2	$S_2O_6^{2-}$	$S_5O_6^{2-}$
CH_4	HF	H_2	NO_3^-	NaHS	SO_3^{2-}	$S_2O_8^{2-}$	
CN^-	HF^{2-}	H_2CO_3	N_2	NaOH	SO_4^{2-}	S_3^{2-}	
Cl^-	HO_2^-	H_2O	Na^+	$NaSO_4^-$	S_2^{2-}	$S_3O_6^{2-}$	
F^-	HS^-	H_2S	$NaCO_3^-$	OH^-	$S_2O_3^{2-}$	S_4^{2-}	
H^+	HSO_3^-	NH_3	NaCl	O_2	$S_2O_4^{2-}$	$S_4O_6^{2-}$	
HCO_3^-	HSO_4^-	NH_4^+	NaF	S^{2-}	$S_2O_5^{2-}$	S_5^{2-}	
Gas species[b]							
C	CH_2	CS_2	ClCN[e]	$(HF)_2$	NCO[e]	N_3[h]	SO_2Cl_2
CCl	CH_2ClF	C_2	ClF	$(HF)_3$	NF[f]	O	SO_2F_2
$CClF_3$	CH_2Cl_2	C_2Cl_2	ClF_3	$(HF)_4$	NF_2[f]	OH	SO_3
CCl_2	CH_2F_2	C_2Cl_4	ClF_5	$(HF)_5$	NF_3[f]	ONCl[i]	SSF_2
CCl_2F_2	CH_2O	C_2Cl_6	ClF_5S	$(HF)_6$	NH[g]	ONF[e]	S_2
CCl_3	CH_3	C_2F_2	ClO	$(HF)_7$	NH_2[g]	O_2	S_2Cl
CCl_3F	CH_3Cl	C_2F_4	ClO_2	HNCO[h]	NH_3[g]	O_3	S_2Cl_2
CCl_4	CH_3F	C_2F_6	ClO_3F	HNO[e]	NO[c]	S	S_2F_{10}
CF	CH_4	C_2HCl	Cl_2O	HNO_2 − cis[e]	NO_2[c]	SCl	S_2O
CF_2	CN[d]	C_2HF	Cl_2	HNO_2 − tra[e]	NO_2Cl[e]	$SClF_5$	S_3
CF_3	CNC[e]	C_2H_2	F	HNO_3[e]	NO_3[c]	SCl_2	S_4
CF_3OF	CNN[e]	C_2H_4	FO	HO_2	NS[j]	SF	S_5
CF_3CN[e]	CO	C_2H_4O	FO_2	HS	N_2[c]	SF_2	S_6
CF_4	COCl	C_2H_6	FS_2F	HSO_3F	N_2F_2-*cis*[f]	SF_3	S_7
CH	COClF	C_2N_2[k]	F_2	H_2	N_2F_2-*trans*[f]	SF_4	S_8
CHCl	$COCl_2$	C_3	F_2O	H_2O	N_2F_4[f]	SF_5	
$CHClF_2$	COF	C_3O_2	H	H_2O_2	N_2H_2-*cis*[e]	SF_6	
$CHCl_2F$	COF_2	C_4	HCN[e]	H_2S	N_2H_4[f]	SO	
$CHCl_3$	COS	C_4N_2[e]	HCO	H_2SO_4	N_2O[c]	$SOCl_2$	
CHF	CO_2	C_5	HCl	H_2S_2	N_2O_3[c]	SOF_2	
CHFO	CS	C_6H_6	HClO	N[c]	N_2O_4[c]	SO_2	
CHF_3	CSF_8	Cl	HF	NCN[h]	N_2O_5[c]	SO_2ClF	
Solid and liquid phases[b]							
Graphite[a]	$Na_2O_{(s)}$[a]	$S_{(monoclinic)}$					
Halite[a]	$S_{(liquid)}$	$S_{(orthorhombic)}$					

[a] Thermochemical data from Johnson et al. (1992).
[b] Thermochemical data mostly from Symonds and Reed (1993), except as noted; other sources listed below.
[c] Pankratz, 1982.
[d] Pankratz et al., 1984.
[e] Stull and Prophet, 1971.
[f] Pankratz, 1984.
[g] Chase et al., 1982.
[h] Chase et al., 1974.
[i] Chase et al., 1975.
[j] Pankratz et al., 1987.
[k] Barin and Knacke, 1973.

modeling nonideal mixing of gases (Spycher and Reed, 1988), but we treat the gases ideally to be consistent with the current capability of GASWORKS. Moreover, gas ideality is a reasonable assumption for the low pressures (≤5 MPa) considered in this study. GASWORKS computes heterogeneous chemical equilibria in gas–solid systems during processes of heating (or cooling), pressure changes, gas–gas mixing, and gas–rock reaction. The program solves simultaneously a series of mass balance, mass

action, and enthalpy balance equations using the basic formulations of CHILLER (Reed, 1982, 1998) modified for gases (Symonds and Reed, 1993).

To avoid small differences in the thermochemical data for the shared species in CHILLER and GASWORKS, we developed a uniform data base for this project. Table 2 summarizes the species used for the gas–water modeling in this paper. Thermochemical data for the aqueous species come from SUPCRT92 (Johnson et al., 1992), whereas thermochemical data for gas species are from GASTHERM (Symonds and Reed, 1993), except as noted in Table 1. In the rock-reaction calculations (case 7), we added aqueous and mineral species from SUPCRT92 (Johnson et al., 1992; Reed (1998) for the major rock-forming elements.

The temperature of the mixture of hot gas and cold water was computed assuming the enthalpy of the mixture equals the sum of the enthalpies of the components, ignoring heat of mixing effects. The equation from Spycher and Reed (1988) to calculate the enthalpy of the mixture is as follows:

$$H_{\mathrm{mix}} = \sum_{i=1}^{n} n_i H_i^{\mathrm{l}} + \sum_{j=1}^{n} n_j H_j^{\mathrm{g}}, \tag{3}$$

where H_{mix} is the total enthalpy of the mixture at a given temperature and pressure, n_i and H_i^{l} are the molar amount and partial molar enthalpy of pure component i in the cold aqueous phase, respectively, and n_j and H_j^{g} are the molar amount and partial molar enthalpy of species j in the high-temperature gas phase, respectively. We assume that the enthalpy of water approximates the enthalpy of the aqueous phase and neglect H_i^{l} values for the aqueous species. Values for H_i^{l} (for water) and H_j^{g} (for individual gas species) were calculated from polynomial equations (e.g., Pankratz, 1982). Both CHILLER and GASWORKS compute the enthalpy of a given composition at a specified temperature and pressure. Hence, we used these programs to fix pressure and solve for the temperature at which the equilibrium composition's enthalpy equals H_{mix}.

2.4. Case 1: Merapi gas–ASW reaction 0.1 MPa

In case 1, we numerically add 915°C Merapi gas to 1 kg of 25°C ASW at 0.1 MPa constant pressure (Figs. 3 and 4). The calculations proceed from 0.0002 to 100 kg of gas added (kga). Note that in this case, kga also equals the g/w mass ratio. The computed mixture is initially liquid-only, then liquid-plus-gas, then gas-only, as temperature increases from 25° to 900°C (Fig. 3a). At <0.008 kga, all the gas species either dissolve as aqueous complexes or precipitate as sulfur (see below). At between 0.008 and 1.7 kga, the mixture consists of both liquid and gas, and the percentage of gas increases from 0.003 to >97% (Fig. 3b).

As the acidic volcanic gas is added to the ASW, the pH of the aqueous solution decreases from ~3.5 at 0.0002 kga to about −0.5 at 1.7 kga (Fig. 3c). The pH decrease is caused mostly by scrubbing of $SO_{2(g)}$ and $HCl_{(g)}$. $SO_{2(g)}$ dissolves by the following disproportionation reaction at <0.03 kga:

$$4SO_{2(g)} + 4H_2O_{(aq)} \rightarrow 3SO_{4(aq)}^{2-} + 6H_{(aq)}^{+} + H_2S_{(aq)}, \tag{4}$$

and at 0.03–1.7 kga:

$$4SO_{2(g)} + 4H_2O_{(aq)} \rightarrow 3HSO_{4(aq)}^{-} + 3H_{(aq)}^{+} + H_2S_{(aq)}, \tag{5}$$

which are driven to the right as the magmatic gas is added to solution. (The arrows in reactions (4) and (5) and in subsequent reactions indicate a process driven to the right by change in composition, pressure, or temperature.) $HCl_{(g)}$ is scrubbed by the reaction:

$$HCl_{(g)} \rightarrow H_{(aq)}^{+} + Cl_{(aq)}^{-}. \tag{6}$$

Fig. 3d shows the main aqueous species of C, Cl, and F. The dominant aqueous species of C is $H_2CO_{3(aq)}$ due to scrubbing of $CO_{2(g)}$ under acidic conditions:

$$CO_{2(g)} + H_2O_{(aq)} \rightarrow H_2CO_{3(aq)}, \tag{7}$$

The molality of $H_2CO_{3(aq)}$ increases until 0.008 kga after which it decreases as most of the $CO_{2(g)}$ exsolves from solution (see below). $Cl_{(aq)}^{-}$ from reaction (6) is the dominant aqueous species of Cl throughout the liquid and liquid-plus-gas regions of the calculations, although $HCl_{(aq)}$ becomes a significant minor species just before the solution boils to dryness due to pH dropping below 1. Scrubbing of $HF_{(g)}$ produces $F_{(aq)}^{-}$ at <0.003 kga:

$$HF_{(g)} \rightarrow H_{(aq)}^{+} + F_{(aq)}^{-}, \tag{8}$$

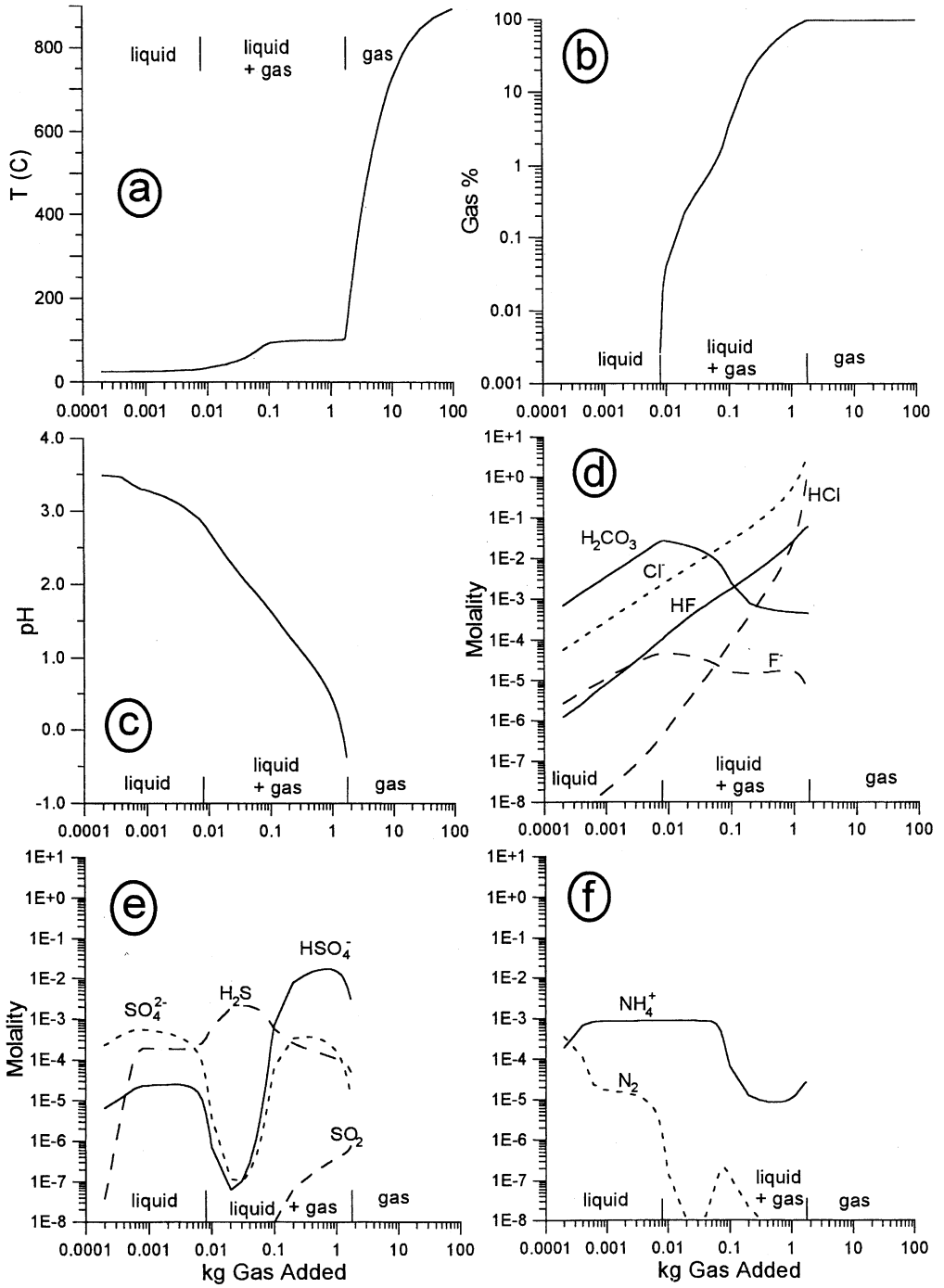

Fig. 3. Diagram showing the results from reacting the 915°C Merapi gas with 25°C ASW at 0.1 MPa (case 1, Fig. 2). In this figure, we show the resulting: (a) mixture temperature; (b) weight percentage of gas in the mixture; (c) pH of the aqueous phase; and (d)–(f) molalities of the dominant aqueous species of C, Cl, F, S, and N. Horizontal axes show the kg of gas added to 1 kg of ASW, which also equals the gas/water ratio.

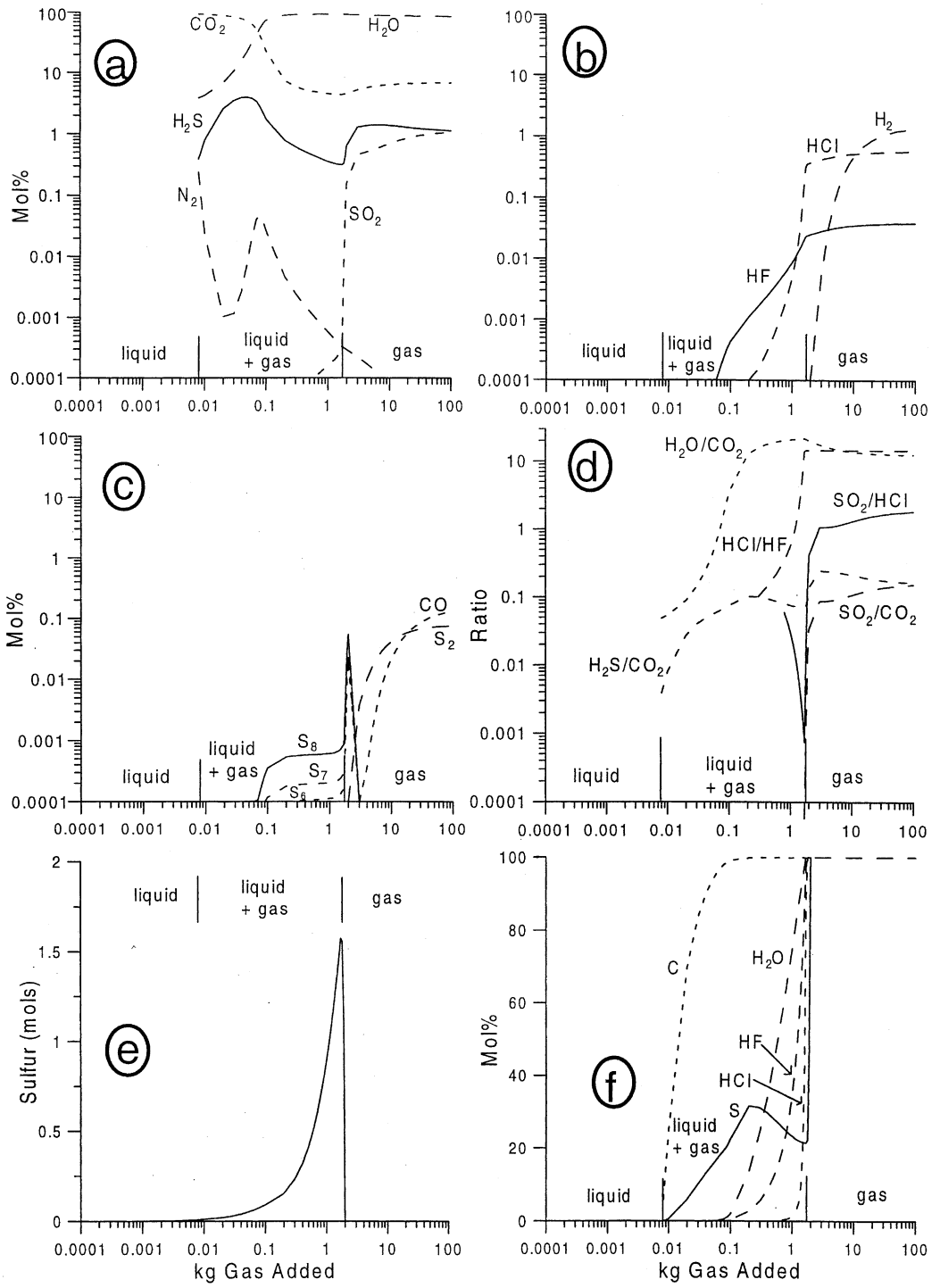

Fig. 4. Diagram showing the results from case 1 calculations (continued from Fig. 3). In this figure, we show the resulting: (a)–(c) mol% values of the major and minor gas species of H, O, C, S, Cl, F, and N; (d) ratios of selected gas species (only plotted when mol% values of both species in ratio exceed 0.0001 mol%); (e) the moles of precipitated sulfur; and (f) mol% of magmatic C ($CO_{2(g)}$ + $CO_{(g)}$), S ($SO_{2(g)}$ + $H_2S_{(g)}$ + $S_{2(g)}$), $H_2O_{(g)}$, $HCl_{(g)}$, and $HF_{(g)}$ that exist in the gas portion of the gas–liquid–solid mixture. Horizontal axes show the kg of gas added to 1 kg of ASW, which also equals the gas/water ratio.

and $HF_{(aq)}$ at 0.003–1.7 kga:

$$HF_{(g)} \rightarrow HF_{(aq)}. \quad (9)$$

The transition from $F^-_{(aq)}$ to $HF_{(aq)}$ is caused by pH dropping to <3.1. The molalities of $Cl^-_{(aq)}$ and fluoride ($F^-_{(aq)} + HF_{(aq)}$) increase through the liquid and liquid-plus-gas regions due to effective scrubbing of $HCl_{(g)}$ and $HF_{(g)}$.

Fig. 3e shows that the most abundant aqueous species of S are $SO^{2-}_{4(aq)}$ (<0.009 kga), $H_2S_{(aq)}$ (0.009–0.1 kga), and $HSO^-_{4(aq)}$ (0.2–1.7 kga). Other aqueous species of S, including polythionates (Table 1), are insignificant. The aqueous speciation of S is complex and depends on several competing processes. Scrubbing of $SO_{2(g)}$ produces three times more $SO^{2-}_{4(aq)}$ or $HSO^-_{4(aq)}$ than $H_2S_{(aq)}$ by reactions (4) and (5). However, scrubbing of $H_{2(g)}$ reduces much of this sulfate to $H_2S_{(aq)}$ by the following reaction at <0.03 kga:

$$SO^{2-}_{4(eq)} + 2H^+_{(aq)} + 4H_{2(g)} \rightarrow H_2S_{(aq)} + 4H_2O_{(aq)}, \quad (10)$$

and its $HSO^-_{4(aq)}$ equivalent at 0.03–1.7 kga. Reduction of sulfate by $H_{2(g)}$ scrubbing is significant because the Merapi 79-2 sample contains 1.54 mol% $H_{2(g)}$ (Table 1), which is common in >900°C volcanic gases (Symonds et al., 1994). Another significant source of $H_2S_{(aq)}$ is $H_2S_{(g)}$ scrubbing:

$$H_2S_{(g)} \rightarrow H_2S_{(aq)}, \quad (11)$$

which occurs throughout the liquid-only and liquid-plus-gas regions. Scrubbing of $CO_{(g)}$ and $S_{2(g)}$ also provide minor contributions to the overall abundance of $H_2S_{(aq)}$ by the following reactions at <0.03 kga:

$$4CO_{(g)} + SO^{2-}_{4(aq)} + 2H^+_{(aq)} + 4H_2O_{(aq)} \rightarrow H_2S_{(aq)} + 4H_2CO_{3(aq)}, \quad (12)$$

$$2S_{2(g)} + 4H_2O_{(aq)} \rightarrow SO^{2-}_{4(aq)} + 2H^+_{(aq)} + 3H_2S_{(aq)}, \quad (13)$$

and their $HSO^-_{4(aq)}$ equivalents at 0.03–1.7 kga. The sum of reactions (4), (5), and (10)–(13) produce a solution dominated by $H_2S_{(aq)}$ rather than $SO^{2-}_{4(aq)}$.

However, at <0.002 kga, significant amounts of $H_2S_{(aq)}$ are oxidized by $N_{2(aq)}$ and $O_{2(aq)}$ in the original ASW yielding sulfate:

$$4N_{2(aq)} + 2H^+_{(aq)} + 3H_2S_{(aq)} + 12H_2O_{(aq)} \rightarrow 8NH^+_{4(aq)} + 3SO^{2-}_{4(aq)}, \quad (14)$$

$$H_2S_{(aq)} + 2O_{2(aq)} \rightarrow SO^{2-}_{4(aq)} + 2H^+_{(aq)}. \quad (15)$$

Reactions (14) and (15) cause $SO^{2-}_{4(aq)}$ to prevail over $H_2S_{(aq)}$ at <0.002 kga. But at 0.0008 kga precipitation of sulfur (see below) also affects sulfur speciation by removing three times more $H_2S_{(aq)}$ than sulfate:

$$SO^{2-}_{4(aq)} + 2H^+_{(aq)} + 3H_2S_{(aq)} \rightarrow 4S_{(s)} + 4H_2O_{(aq)}. \quad (16)$$

Sulfur precipitation is the main reason that $SO^{2-}_{4(aq)}$ continues to prevail over $H_2S_{(aq)}$ between 0.002 and 0.005 kga. However, between 0.005 and 0.02 kga, the dropping pH (Fig. 3c) drives reaction (16) to the right, consuming increasing amounts of $SO^{2-}_{4(aq)}$ until almost all available $SO^{2-}_{4(aq)}$ precipitates as sulfur at 0.02 kga. However, between 0.02 and 0.7 kga, the percentage of sulfur degassed as $H_2S_{(g)}$ increases substantially (see below); this decreases the supply of $H_2S_{(aq)}$ for reaction (16), allowing $SO^{2-}_{4(aq)}$ and its lower-pH equivalent, $HSO^-_{4(aq)}$, to increase; in effect, sulfur precipitation and $H_2S_{(g)}$ degassing oxidize the remaining liquid.

A right-shift in reaction (14) causes $NH^+_{4(aq)}$ to prevail over $N_{2(aq)}$ as the main aqueous N species (Fig. 3f). The concentration of $NH^+_{4(aq)}$ remains relatively constant until >0.05 kga when it declines significantly due to substantial $N_{2(g)}$ degassing (see below) by the reaction:

$$8NH^+_{4(aq)} + 3HSO^-_{4(aq)} \rightarrow 4N_{2(g)} + 5H^+_{(aq)} + 3H_2S_{(aq)} + 12H_2O_{(aq)}, \quad (17)$$

which follows the concentration of $HSO^-_{4(aq)}$ (Fig. 3e). Nitrogen necessarily derives entirely from the ASW because the Merapi gas analysis by Le Guern et al. (1982) is insufficient to determine the concentration of nonatmospheric $N_{2(g)}$. Nonetheless, many convergent-plate volcanoes discharge gases with excess $N_{2(g)}$ (e.g. $N_{2(g)}/Ar_{(g)}$ ratios that exceed air and ASW; Matsuo et al., 1978) that would also affect $NH^+_{4(aq)}$.

At the onset of gas formation at 0.008 kga (Fig. 3b) where $T = 31.8$°C and pH = 2.8, the gas phase is dominated by $CO_{2(g)}$, $H_2O_{(g)}$, $H_2S_{(g)}$, and

$N_{2(g)}$ (Fig. 4a); the abundances of $CO_{2(g)}$, $H_2S_{(g)}$, and $N_{2(g)}$ reflect their low solubilities in water. Proceeding across the liquid-plus-gas region there are several trends: (1) the mol% of $H_2O_{(g)}$ increases with temperature; (2) the mol% of $CO_{2(g)}$ decreases due to dilution with $H_2O_{(g)}$; (3) the mol% of $H_2S_{(g)}$ first increases in concert with $H_2S_{(aq)}$ (Fig. 3e) and then decreases mostly due to dilution effects; and (4) the mol% of $N_{2(g)}$ shows a net decrease following $N_{2(aq)}$ (Fig. 3f). Minor amounts (>0.0001 mol%) of $HF_{(g)}$ form at 0.06 kga and it increases loglinearly to near-magmatic levels at 1.7 kga (Fig. 4b). In contrast, it takes 0.2 kga for $HCl_{(g)}$ to exceed 0.0001 mol%, but at >0.2 kga, the $HCl_{(g)}$ concentration increases at an accelerating rate, following the steeper decline in pH (especially at pH < 1), until reaching near-magmatic levels at 1.7 kga (Figs. 3c and 4b). Minor sulfur species in the liquid-plus-gas region include $S_{8(g)}$ and $S_{7(g)}$ (Fig. 4c) at >0.07 and >0.09 kga, respectively, but $SO_{2(g)}$ remains insignificant as long as liquid is present (Fig. 4a). $H_{2(g)}$ is also insignificant in the liquid-plus-gas region (Fig. 4b) as it participates heavily in the reduction of $SO^{2-}_{4(aq)}$ (reaction 10).

When the liquid phase boils dry at 1.8 kga ($T = \sim 106°C$), the concentration of $SO_{2(g)}$ increases by several orders of magnitude (Fig. 4a). Concentrations of $S_{8(g)}$ and $S_{7(g)}$ also increase sharply at 1.8 kga and peak at 2.0 kga (Fig. 4c) coincident with the transition of precipitated sulfur from orthorhombic to liquid sulfur and the evaporation of liquid sulfur (Fig. 4e), respectively. Shortly beyond 2 kga, $S_{8(g)}$ and $S_{7(g)}$ decline abruptly (Fig. 4c). $H_{2(g)}$, $S_{2(g)}$, and $CO_{(g)}$ also become significant minor species at >2–3 kga (Fig. 4b and c). As still more gas is added, the concentrations (Fig. 4a–c) and ratios (Fig. 4d) of individual gas species and the temperature of the gas mixture (Fig. 3a) approach magmatic values.

Significant amounts of solid or liquid native sulfur form at between 0.0008 and 1.9 kga by reaction (16) at <0.03 kga and its $HSO^{-}_{4(aq)}$ equivalent at 0.03–1.7 kga (Fig. 4e). At >1.9 kga, S exists only in the gaseous state. Precipitation of sulfur scrubs more $SO_{2(g)}$ and $H_2S_{(g)}$ than hydrolysis over much of the liquid and liquid-plus-gas regions.

In summary, as the system dries out across the liquid-plus-gas region, the evolved gas progresses (in order of abundance) from $CO_{2(g)}$–$H_2O_{(g)}$–$H_2S_{(g)}$–$N_{2(g)}$ to $H_2O_{(g)}$–$CO_{2(g)}$–$H_2S_{(g)}$. Drying out across the liquid-plus-gas region is also characterized by: (1) dramatic increases in the $H_2O_{(g)}/CO_{2(g)}$ and $H_2S_{(g)}/CO_{2(g)}$ between 0.008 and ~0.2 kga; (2) a large increase in $HCl_{(g)}/HF_{(g)}$ between 0.3 and 1.7 kga; and (3) a steep decline in $SO_{2(g)}/HCl_{(g)}$ between 0.8 and 1.7 kga due to the enhanced exsolution of $HCl_{(g)}$ from acidic solutions (Fig. 4d). As the calculations progress into the gas-only region at 1.8 kga, significant concentrations of $SO_{2(g)}$ finally enter the gas phases and $SO_{2(g)}/HCl_{(g)}$, $SO_{2(g)}/CO_{2(g)}$, and $SO_{2(g)}/H_2S_{(g)}$ (not shown) increase dramatically (Fig. 4d).

Fig. 4f shows the efficiency of the gas-water reaction on scrubbing magmatic $H_2O_{(g)}$, C ($CO_{2(g)}$ + $CO_{(g)}$), S ($SO_{2(g)}$, + $H_2S_{(g)}$ + $S_{2(g)}$), $HCl_{(g)}$, and $HF_{(g)}$. Magmatic $CO_{2(g)}$ and $CO_{(g)}$ show the most resistance to scrubbing. $CO_{2(g)}$ and $CO_{(g)}$ are scrubbed effectively in the liquid-only region by reactions (7) and (12), respectively. However, as the calculations progress across the liquid-plus-gas region (0.008–0.3 kga), the amount of carbon that exists as $CO_{2(g)}$ increases from ~2 to ~100%.

$SO_{2(g)}$, $S_{2(g)}$, and, to a lesser extent, $H_2S_{(g)}$ are more affected by scrubbing than is $CO_{2(g)}$. Between 0.002 and 1.8 kga, the majority of the added $SO_{2(g)}$, $H_2S_{(g)}$, and $S_{2(g)}$ precipitates as native sulfur (Fig. 4e) by reaction (16). Hydrolysis is also effective at scrubbing substantial amounts of $SO_{2(g)}$ (reactions (4) and (5)), $H_2S_{(g)}$ (reaction (11)), and $S_{2(g)}$ (reaction (13)) in the liquid and liquid-plus-gas regions, especially at <0.002 kga. Despite sulfur precipitation and hydrolysis, up to ~32% of total added sulfur discharges as $H_2S_{(g)}$ in the liquid-plus-gas region.

More than 99% of the magmatic $H_2O_{(g)}$ condenses into the liquid phase until midway through the liquid-plus-gas region (0.09 kga); after which an increasing amount of water boils as temperature approaches and then exceeds 100°C. Over 99% of $HF_{(g)}$ is scrubbed by reactions (8) and (9). But at >0.1 kga, a growing amount of $HF_{(g)}$ boils into the gas phase. Similarly, >99% of $HCl_{(g)}$ is scrubbed by reaction (6) until, at >0.9 kga, pH drops below 1, reaction (6) shifts to the left, and an escalating amount of $HCl_{(g)}$ exsolves from solution. Finally, $H_{2(g)}$ participates readily in aqueous sulfur redox equilibria and is effectively scrubbed throughout the liquid and liquid-plus-gas regions.

2.5. Case 2: closed-system cooling of Merapi gas at 0.1 MPa

In the case 2 calculations, we examine the effect of the ASW in case 1 by cooling the Merapi gas (Table 1) from 895 to 1°C at 0.1 MPa, and comparing the results to the temperature range (895–25°C) of the case 1 calculations. Instead of narrating the details of case 2, we focus on significant similarities and differences between the two cases. First, despite the absence of ASW, a liquid phase forms when the Merapi gas cools below ~100°C. This process mimics the formation of acidic condensates by cooling volcanic gases (Stoiber and Rose, 1970). Second, as in case 1, sulfur precipitates at $T \leq 188.3$°C. Third, both cases show similar concentrations of the main gas species in the liquid-plus-gas region except that: (1) the liquid-plus-gas region extends from ~106° to ~32°C in case 1 and from ~100°C to the freezing point of the liquid in case 2; and (2) $H_2S_{(g)}$, $HF_{(g)}$, and $HCl_{(g)}$ are more abundant in case 2 (Fig. 5); both trends reflect less water and, therefore, less effective scrubbing in case 2 than in case 1.

Fourth, comparison of the two cases in the gas-only region highlights the impact of ASW on case 1. Both cases show virtually identical concentrations of the main gas species at 895°C (Fig. 5) where case 1 has a very high g/w ratio (Fig. 3a). However, as temperature decreases from 895 to ~106°C, ASW-dilution effects in case 1 produce progressively higher concentrations of $H_2O_{(g)}$ and lower concentrations of $CO_{2(g)}$, $H_2S_{(g)}$, $HCl_{(g)}$, and $HF_{(g)}$ than in case 2 (Fig. 5). Cooling in both cases drives the production of $H_2S_{(g)}$ from $SO_{2(g)}$ by the following reaction:

$$SO_{2(g)} + 3H_{2(g)} \rightarrow H_2S_{(g)} + 2H_2O_{(g)}. \quad (18)$$

Cooling therefore provides another mechanism of depleting $SO_{2(g)}$ and $H_{2(g)}$ in magmatic gases. The $SO_{2(g)}$ concentration is lower in case 1 between 895 and ~270°C due to dilution effects, but higher in case 1 than in case 2 between ~270 and ~106°C because the higher $H_2O_{(g)}$ concentrations in case 1 produce a smaller right-shift in reaction (18). Fifth, the case 2 results are obviously unaffected by addition of air components ($N_{2(aq)}$ and $O_{2(aq)}$) in the ASW prevailing in case 1.

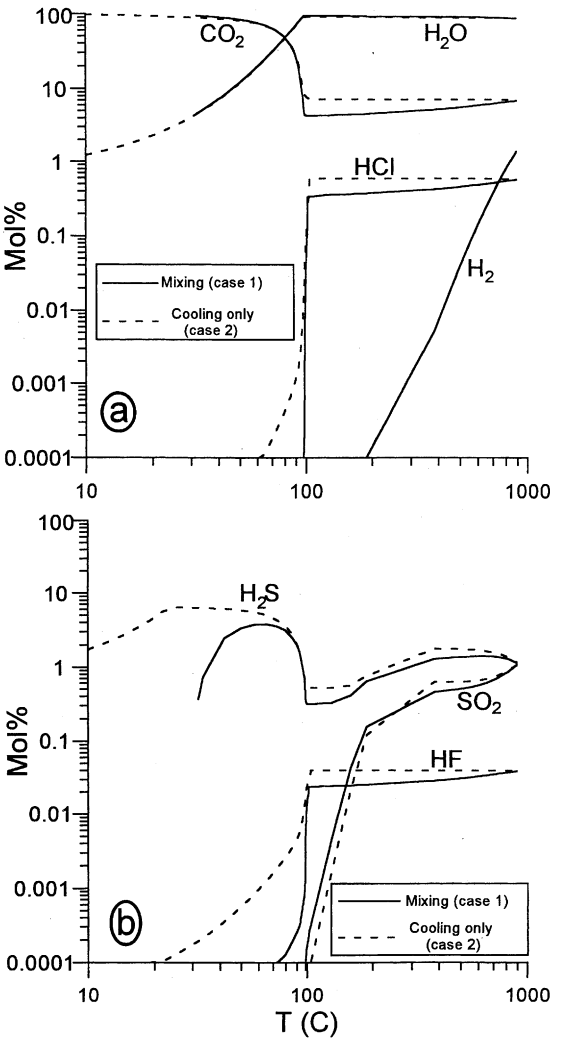

Fig. 5. Diagram comparing concentrations of selected gas species from the Merapi gas–ASW mixing calculations (case 1; Figs. 3 and 4) with the corresponding results for simple closed-system cooling of the Merapi gas (case 2, Fig. 2). For comparison with Figs. 3 and 4, the liquid-plus-gas region for the case 1 calculations is between ~32 and ~106°C. The liquid-plus-gas region for the case 2 calculations extends from ~100°C to the freezing point of the liquid phase.

2.6. Case 3: Merapi gas–ASW reaction at 5 MPa

In case 3, we investigate the influence of a much higher pressure (5 MPa) on the processes defined in the lower pressure case 1 calculations. The case 3 results (Figs. 6 and 7) are broadly similar to those of case 1, but important differences between the runs are

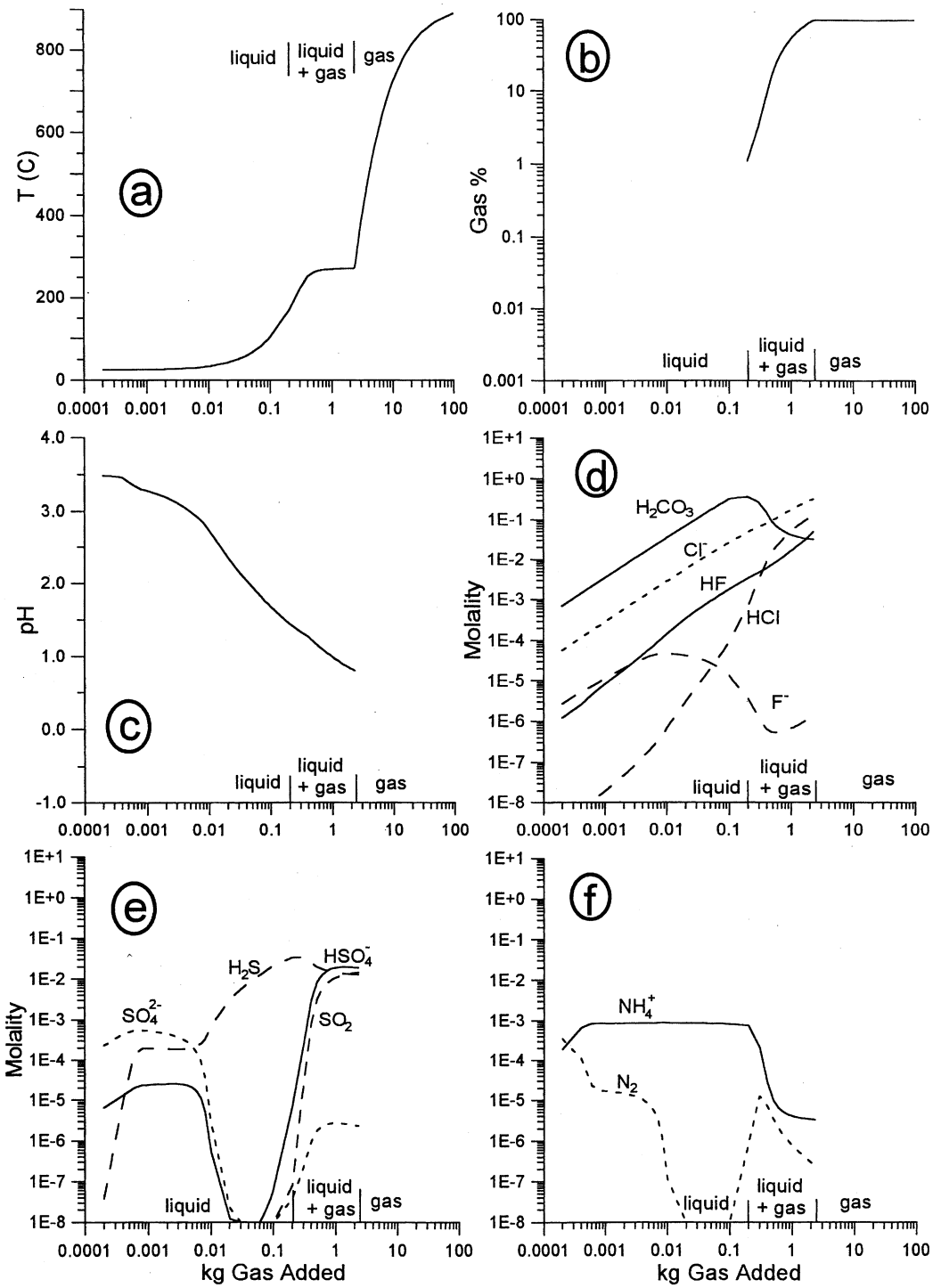

Fig. 6. Diagram showing the results from reacting the 915°C Merapi gas with 25°C ASW at 5 MPa (case 3, Fig. 2). In this figure, we show the resulting: (a) mixture temperature; (b) weight percentage of gas in the mixture; (c) pH of the aqueous phase; and (d)–(f) molalities of the dominant aqueous species of C, Cl, F, S, and N. Horizontal axes show the kg of gas added to 1 kg of ASW, which also equals the gas/water ratio.

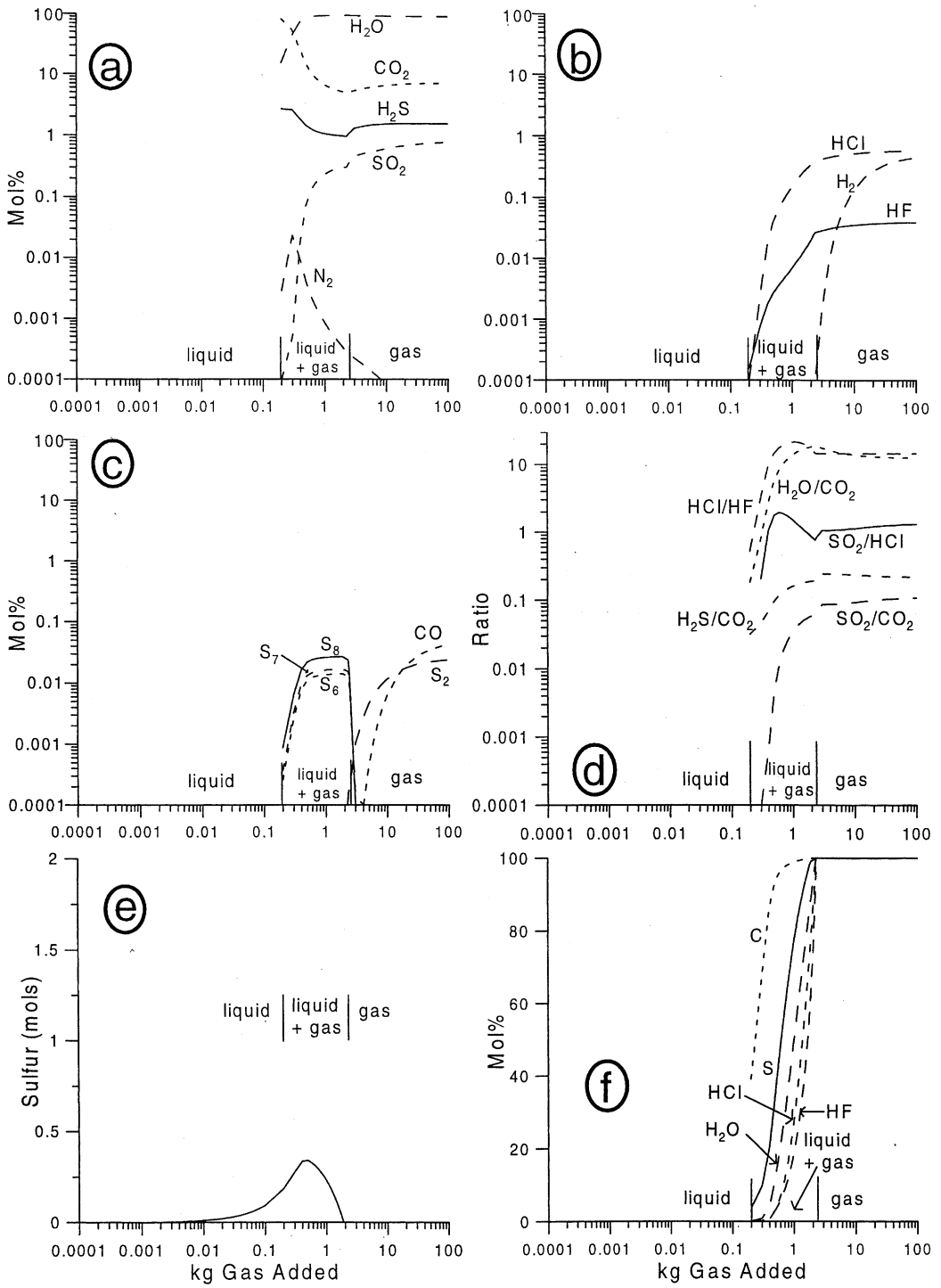

Fig. 7. Diagram showing the results from the case 3 calculations (continued from Fig. 6). In this figure, we show the resulting: (a)–(c) mol% values of the major and minor gas species of H, O, C, S, Cl, F, and N; (d) ratios of selected gas species (only plotted when mol% values of both species in ratio exceed 0.0001 mol%); (e) the moles of precipitated sulfur; and (f) mol% of magmatic C ($CO_{2(g)}$ + $CO_{(g)}$), S ($SO_{2(g)}$ + $H_2S_{(g)}$ + $S_{2(g)}$), $H_2O_{(g)}$, $HCl_{(g)}$, and $HF_{(g)}$ that exist in the gas portion of the gas–liquid–solid mixture. Horizontal axes show the kg of gas added to 1 kg of ASW, which also equals the gas/water ratio.

as follows: First, at 5 MPa the mixture requires considerably more enthalpy to boil than at 0.1 MPa, thus the liquid-only region expands to between 0.0002 and <0.2 kga as it requires more added gas and higher temperatures to induce boiling (Fig. 6a). Second, at <0.1 kga, the pHs and $Cl^-_{(aq)}$ concentrations in cases 1 and 3 are similar, but at >0.1 kga, the case 3 pH and $Cl^-_{(aq)}$ concentration become progressively higher and lower, respectively (Figs. 3c and d and 6c and d), coinciding with the temperature increase in case 3 (Fig. 6a) from 104° (0.1 kga) to 273°C (2.3 kga). These trends mostly originate from the 4-orders-of-magnitude decrease in the equilibrium constant for reaction (6) as temperature increases from 104° to 273°C, a direct consequence of the simultaneous decrease in the dielectric constant of water. Third, $H_2CO_{3(aq)}$ and $H_2S_{(aq)}$ reach much higher concentrations in case 3 than in case 1 (Figs. 3d and e and 6d and e); this reflects the higher solubilities of $CO_{2(g)}$, $SO_{2(g)}$, $H_2S_{(g)}$, $H_{2(g)}$, $S_{2(g)}$, and $CO_{(g)}$ at higher pressures by reactions (4), (5), (7), and (10)–(13). Fourth, in case 3, $SO_{2(aq)}$ becomes a significant aqueous species of sulfur in the liquid-plus-gas region (Fig. 6e).

Fifth, the concentrations of $SO_{2(g)}$ and the ratios of $SO_{2(g)}/HCl_{(g)}$, $SO_{2(g)}/H_2S_{(g)}$ (not shown), and $SO_{2(g)}/CO_{2(g)}$ in the liquid-plus-gas region for case 3 (Fig. 7a and d) greatly exceed those for case 1 (Fig. 4a and d). These surprising results suggests that, within the liquid-plus-gas region at higher pressures, $SO_{2(g)}$ is less susceptible to scrubbing (Fig. 7f) and can become a significant minor species of sulfur behind $H_2S_{(g)}$. In general, higher pressures force more gas to dissolve in solution; hence, the expansion of the liquid-only region in case 3. However, the expansion of the liquid-only region in case 3 produces hotter temperatures (Figs. 6a) in the liquid-plus-gas region than in case 1(Fig. 3a); these higher temperatures allow less sulfur to precipitate (Figs. 7e) and generate the higher concentrations of $SO_{2(g)}$. Incidentally, $O_{2(aq)}$ in the input ASW has little impact on $SO_{2(g)}$ production in case 3 because repeating the calculations with $O_{2(aq)}$-free ASW produces virtually identical $SO_{2(g)}$ concentrations.

Sixth, in the liquid-plus-gas region of case 3 (Fig. 7b, d and f), the concentration of $HCl_{(g)}$ (between 0.2 and 1.6 kga), and the $HCl_{(g)}/HF_{(g)}$ ratio (between 0.2 and 3 kga) exceed the case 1 values (Fig. 4b, d and f), reflecting the left-shift of reaction (6) as discussed above. Finally, in the gas-only region of case 3 (Fig. 7a and b), the concentrations of $SO_{2(g)}$ and $H_{2(g)}$ lag the case 1 values (Fig. 4a and b) because of pressure-induced volume effects that favor fewer moles of gas on the product side of reaction (18) (Gerlach and Casadevall, 1986). Like case 1, trivial amounts of $H_{2(g)}$ exist in the liquid-plus-gas region as it is consumed by aqueous sulfur redox equilibria (reaction (10)).

2.7. Case 4: variations in water temperature

To explore the influence of the ASW temperature on case 1, we repeat the case 1 calculations, but use 50, 99, and 100°C ASW (case 4). The calculations proceed by adding between 0.002 and 100 kg of Merapi gas into 1 kg of ASW at 0.1 MPa. The 50 and 99°C ASW examples explore mixing with higher-temperature liquid and liquid-plus-gas phases, respectively. The 100°C ASW example is an end-member where the ASW has boiled completely.

We emphasize only the resulting gas compositions (Fig. 8). Starting with 50°C ASW (Fig. 8a and b) generates a gas phase broadly similar to the case 1 results (Fig. 4a and b). The main differences are that the liquid-plus-gas region starts at 0.005 kga rather than 0.008 kga in case 1 and that $N_{2(g)}$ concentration exceeds $H_2S_{(g)}$ at first boiling (<0.007 kga) due to a heating-induced right-shift in reaction (17). The 99°C ASW example (Fig. 8c and d) diverges further from the case 1 results. Note in particular that the liquid-plus-gas region extends to the beginning of the calculations (0.0002 kga), $CO_{2(g)}$ never surpasses $H_2O_{(g)}$ at small amounts of gas added as it does in the 25 and 50°C ASW examples (Figs. 4a and 8a), the maximum concentrations of $H_2S_{(g)}$ are smaller than when starting with 25 and 50°C ASW, and that $N_{2(g)}$ exceeds $H_2S_{(g)}$ at <0.008 kga.

Continuing to diverge from case 1, the 100°C ASW example (Fig. 8e and f) is essentially a steam–magmatic gas mixing calculation. Hence, all the magmatic-gas species have low concentrations at the outset. The concentrations of $CO_{2(g)}$, $H_2S_{(g)}$, $HCl_{(g)}$, and $HF_{(g)}$ increase steadily as a function of gas added until they begin to level off at >1 kga. $SO_{2(g)}$ follows a similar trend, but flattens at >3 kga. In contrast to case 1, $SO_{2(g)}$ remains a significant secondary sulfur species at <1.8 kga, $HCl_{(g)}/HF_{(g)}$ always

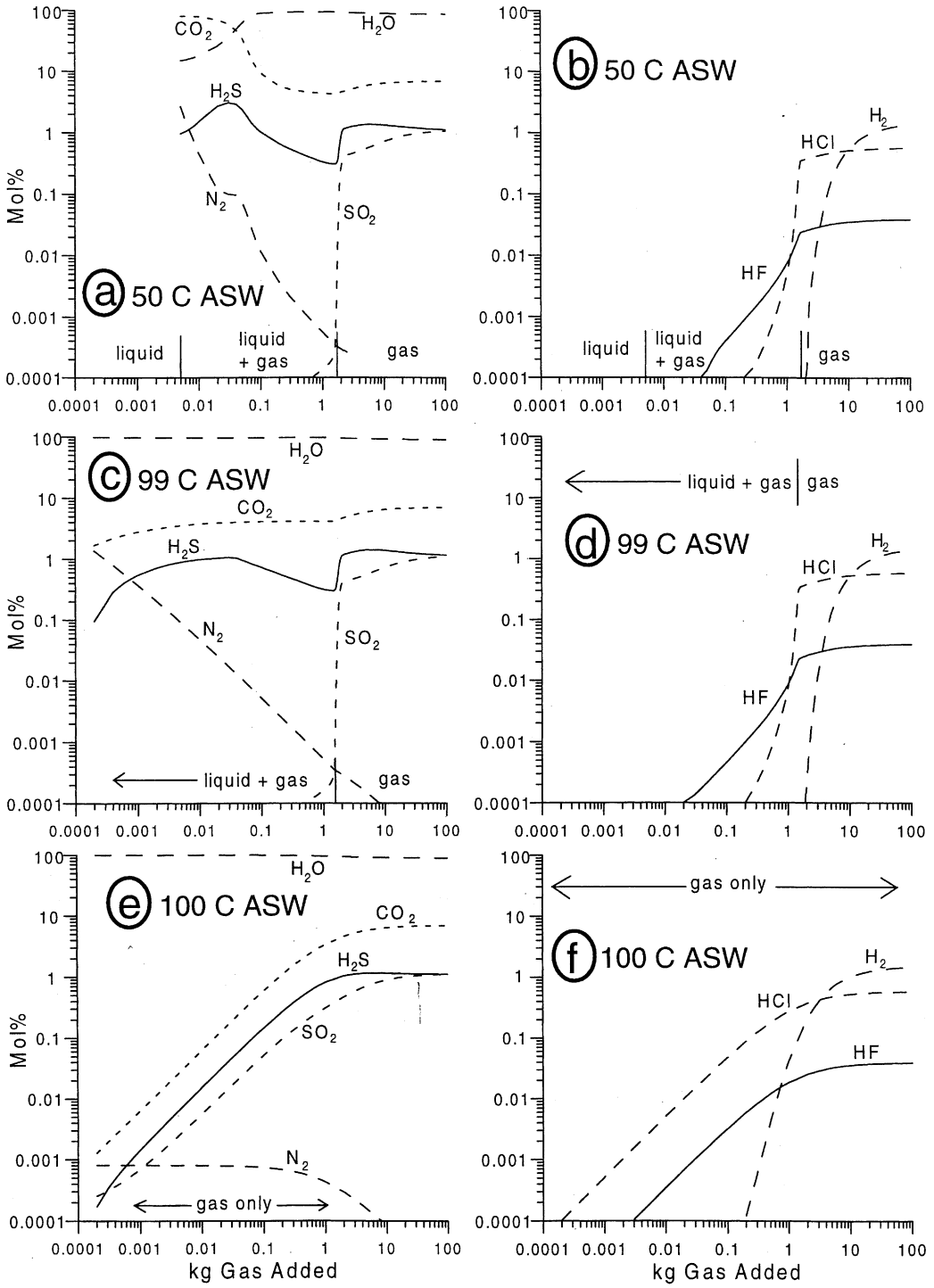

Fig. 8. Diagram showing mol% concentrations of the most abundant gas species of H, O, C, S, Cl, F, and N from reacting the 915°C Merapi gas with (a), (b) 50°; (c), (d) 99°; and (e), (f) 100°C ASW at 0.1 MPa (case 4, Fig. 2). Horizontal axes show the kg of gas added to 1 kg of ASW, which also equals the gas/water ratio.

approximates its ratio (~14.7) in the magmatic gas even at <1.8 kga, and the concentration of $N_{2(g)}$ remains flat at 0.0008 mol% until the added gas significantly dilutes the mixture (>0.1 kga).

2.8. Case 5: variations in water composition

In case 5 we investigate the departure from case 1 caused by changing the input water composition. In this example, we start with three batches of 1 kg ASW plus 0.1 kg of Merapi gas (1.1 kg total) to place these calculations within the liquid-plus-gas region of case 1 (Figs. 3 and 4). Then, we add between 0.001 and 100 g of either $H_2SO_{4(l)}$, $NaCl_{(s)}$, or $NaHCO_{3(s)}$ into each batch to simulate a wide range of acid sulfate, neutral chloride, and bicarbonate waters, respectively, which are the most common volcano waters besides pure ASW (see above). The modeling simulates gas addition into waters containing approximately 1–98,000 ppm $SO^{2-}_{4(aq)}$, 0.6–55,000 ppm $Cl^{-}_{(aq)}$, or 0.7–73,000 ppm $HCO^{-}_{3(aq)}$. Total enthalpy and pressure are fixed at case 1 values (for 0.1 kga) and used to compute temperature at each increment of substance added; hence temperature varies over a small range between 90 and 94°C.

Fig. 9a–f shows the resulting gas compositions as a function of $H_2SO_{4(l)}$, $NaCl_{(s)}$, or $NaHCO_{3(s)}$ added to the input mixture. Addition of <0.1 g of $H_2SO_{4(l)}$ to the input mixture has little effect on the evolved gas composition, but adding more than 0.1 g of $H_2SO_{4(l)}$ causes $H_2S_{(g)}$ to decline by driving reaction (16) to the right, which consumes $H_2S_{(aq)}$ and precipitates sulfur (Fig. 9a). Adding >10 g of $H_2SO_{4(l)}$ to the input mixture also causes a significant increase in $SO_{2(g)}$ concentration by reversing reaction (5). Nonetheless, $H_2S_{(g)}$ remains the dominant sulfur gas even at 100 g $H_2SO_{4(l)}$ added to the input mixture. Adding $H_2SO_{4(l)}$ also causes $HCl_{(g)}$ to increase by acidifying the solution and reversing reaction (6); $HCl_{(g)}$ reaches significant concentrations when additions of $H_2SO_{4(l)}$ exceed 50 g (pH < 0.5; Fig. 9b). This reflects the high exsolution of $HCl_{(g)}$ from extremely acidic solutions, as documented in case 1. Adding $NaCl_{(s)}$ to the input mixture has little effect on the gas composition, except that $HCl_{(g)}$ increases by reversing reaction (6) when additions of $NaCl_{(s)}$ exceed 30 g (Fig. 9c and d).

The main effect of adding $NaHCO_{3(s)}$ to the input mixture is to increase the $HCO^{-}_{3(aq)}$ concentration, which drives the following reaction:

$$HCO^{-}_{3(aq)} + H^{+}_{(aq)} \rightarrow H_2O_{(aq)} + CO_{2(g)}, \quad (19)$$

to the right; this increases pH from 1.6 to 8.3 and the concentration of $CO_{2(g)}$ from 21.4 to 29.7 mol% over the course of the calculations (Fig. 9e). The pH increase diminishes $HF_{(g)}$ by driving reaction (8) to the right (Fig. 9f). The rising pH also causes $H_{2(g)}$ to increase by driving reaction (10) to the left, especially between 5 and 10 g of $NaHCO_{3(s)}$ added when pH increases from 3.3 to 7.2 (Fig. 9f). Finally, at between 0.001 and 8 g of $NaHCO_{3(s)}$ added the pH increase induces dissolution of native sulfur and an increase in $H_2S_{(g)}$ (Fig. 9e) by reversing reaction (16). Further pH increase at >8 g of $NaHCO_{3(s)}$ added lowers $H_2S_{(g)}$ as $H_2S_{(aq)}$ dissociates by the following reaction:

$$H_2S_{(aq)} \rightarrow H^{+}_{(aq)} + HS^{-}_{(aq)}, \quad (20)$$

and, as a consequence, reaction (11) shifts to the right.

2.9. Case 6: variations in magmatic gas composition

In case 6 we explore the effects relative to case 1, of varying the input magmatic-gas composition. In this case we run seven sets of calculations wherein we vary the concentrations of $H_2O_{(g)}$ (30–99.9%), $CO_{2(g)}$ (0.01–50%), $SO_{2(g)}$ (0.001–50%), $H_2S_{(g)}$ (0.001–3%), $HCl_{(g)}$ (0.01–1%), and $HF_{(g)}$ (0.01–0.2%), and oxygen fugacity ($\log fO_2$ from −13 to −5) in the Merapi gas composition to cover their observed ranges in high-temperature magmatic gases (Symonds et al., 1994); the investigated fO_2 ranges, from ~0.5 log units below that controlled by the quartz–fayalite–magnetite (QFM) buffer to about 2 log units above the hematite–magnetite (HM) buffer, include a much higher range of oxidation states than that observed in high-temperature magmatic gases (Symonds et al., 1994). For each calculation step, we change the concentration of the selected species in the Merapi gas and then add 0.1 kg of the modified Merapi gas (at 915°C) to 1 kg of 25°C ASW. We fix pressure at 0.1 MPa to place all these calculations within the liquid-plus-gas region of case 1 (Figs. 3 and 4). Temperature varies widely over the course of these calculations in concert with the broad range of enthalpies for the various gas mixtures. In particular, the enthalpy of $H_2O_{(g)}$ is much greater than the enthalpies of the other gases so the calculated mixture

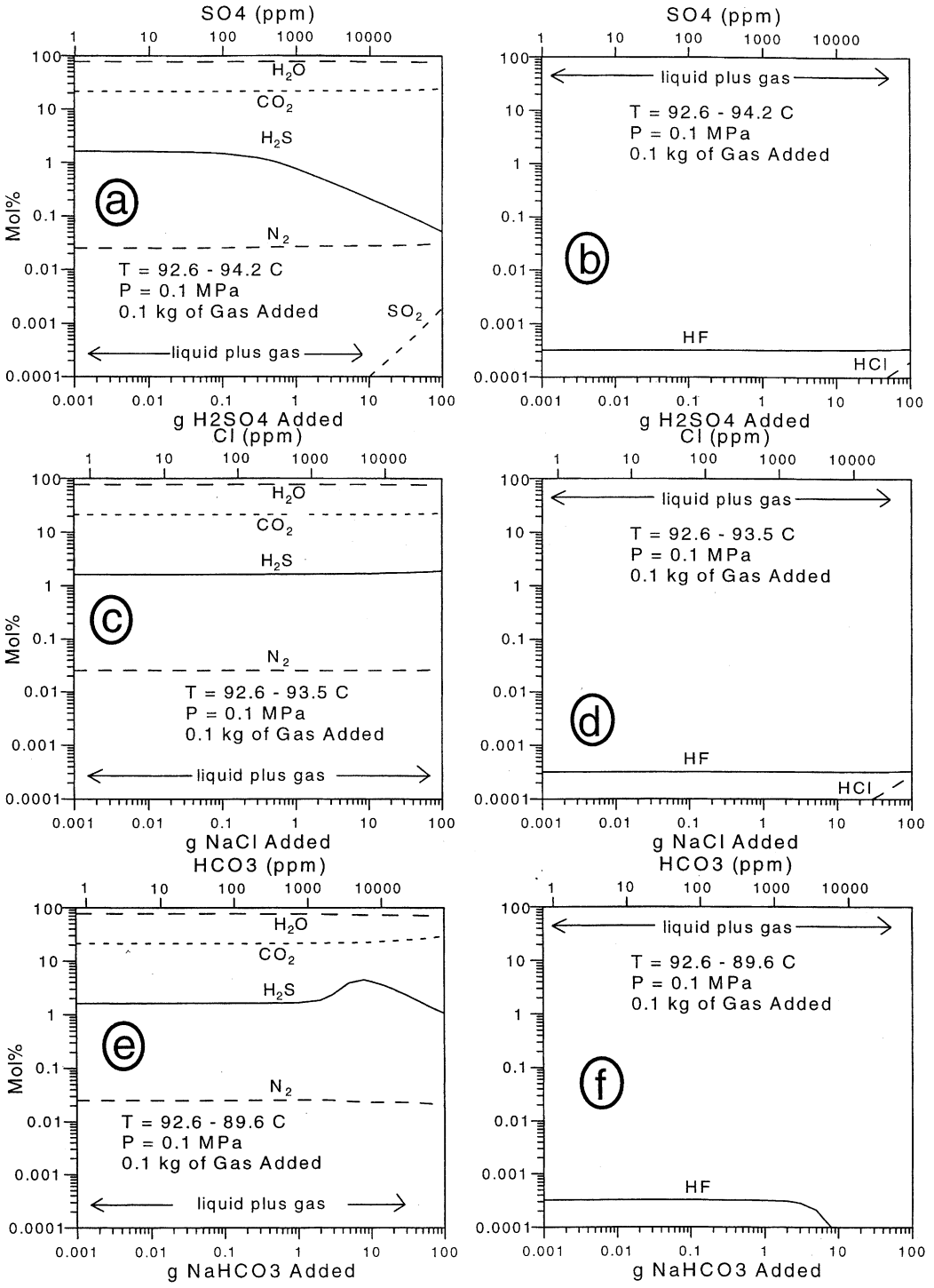

Fig. 9. Diagram showing mol% concentrations of the most abundant gas species of H, O, C, S, Cl, F, and N from reacting 0.1 kg of the 915°C Merapi gas with 1 kg of 25°C ASW containing variables amounts of: (a), (b) $H_2SO_{4(l)}$; (c), (d) $NaCl_{(S)}$; and (e), (f) $NaHCO_{3(s)}$ at 0.1 MPa (case 5, Fig. 2). Bottom horizontal axes show the g of $H_2SO_{4(l)}$, $NaCl_{(S)}$, or $NaHCO_{3(s)}$, respectively, added to 1 kg of ASW; top horizontal axes show the respective concentrations (ppm) of $SO^{2-}_{4(aq)}$, $Cl^{-}_{(aq)}$, or $HCO^{-}_{3(aq)}$ before addition of gas. (Gas/water = 100 g gas/[1000 g ASW + g additive] ≈ 0.1). Temperature range applies as the calculations proceed from left to right on the diagrams.

temperature generally rises or falls in concert with the bulk $H_2O_{(g)}$ concentration in the magmatic gas.

The computed gas compositions for the case 6 calculations are shown in Figs. 10 and 11. Varying the $H_2O_{(g)}$ concentration in the magmatic gas from 30 to 99.9 mol% produces an increase in mixture temperature from 58.0 to 99.7°C, a decrease in $CO_{2(g)}$ and $H_2S_{(g)}$, an increase in $H_2O_{(g)}$ and $N_{2(g)}$, and a slight increase followed by a decrease in $HF_{(g)}$ (Fig. 10a and b). The rise in temperature causes more $H_2O_{(g)}$ to boil into the gas phase. However, dilution of the magmatic gas by $H_2O_{(g)}$ is the main cause for the falling concentrations of $CO_{2(g)}$ and $H_2S_{(g)}$ because much of the injected carbon and sulfur gases reside in the mixture's solid (sulfur) and gaseous phases. Dilution of the magmatic gas also causes $HF_{(g)}$ to decline at >80% $H_2O_{(g)}$ in the magmatic gas, but this is offset at <80% $H_2O_{(g)}$ by the temperature-induced left-shift in reaction (9) and because most of the mixture's fluoride resides as $HF_{(aq)}$, which helps initially to offset dilution effects. Finally, $N_{2(g)}$ increases because the rising temperature and enhanced boiling of the ASW produce a right-shift in reaction (17).

Increasing the magmatic-gas $CO_{2(g)}$ concentration from 0.01 to 50% induces a temperature decrease from 99.0° to 63.8°C along with a drop in $H_2O_{(g)}$, an increase in $CO_{2(g)}$ due to the temperature drop and increased $CO_{2(g)}$ injection, a dilution-induced decrease in $H_2S_{(g)}$, a decrease in $HF_{(g)}$ due to temperature and dilution effects, and a decrease in $N_{2(g)}$ caused by a cooling-induced left-shift in reaction (17) (Fig. 10c and d). Similarly, increasing the magmatic-gas $SO_{2(g)}$ concentration from 0.001 to 50% produces a drop in temperature (from 92.8 to 58.9°C) and a concomitant decrease in $H_2O_{(g)}$, a decrease in $HF_{(g)}$, and an increase in $CO_{2(g)}$ reflecting the decline in $H_2O_{(g)}$ (Fig. 10e and f). However, the $SO_{2(g)}$ increase also produces a sharper drop in $H_2S_{(g)}$ than in the $CO_{2(g)}$ injection run, a direct consequence of sulfur precipitation by reaction (16). The $SO_{2(g)}$ increase also boosts $N_{2(g)}$ by elevating $HSO^-_{4(aq)}$ and driving reaction (17) to the right. The increases in $HSO^-_{4(aq)}$ and $H^+_{(aq)}$ associated with the $SO_{2(g)}$ increases also causes $H_{2(g)}$ to decline by driving reaction (10) to the right. But note that a left-shift in reaction (10) causes $H_{2(g)}$ to increase to significant levels as $SO_{2(g)}$ decreases from 1.15 mol%, the level in the Merapi 79-2 sample, to 0.001 mol%. Finally, $SO_{2(g)}$ itself is only just slightly elevated above 0.0001 mol% between 9 and 26% $SO_{2(g)}$ in the magmatic gas, and remains negligible with respect to $H_2S_{(g)}$. Higher concentrations of $HSO^-_{4(aq)}$ produce the small amounts of $SO_{2(g)}$ by favoring the reactant side of reaction (5). But at >26% $SO_{2(g)}$ in the magmatic gas, falling concentrations of $H_2S_{(aq)}$ as sulfur precipitates offset $HSO^-_{4(aq)}$ production, and $SO_{2(g)}$ declines.

In contrast, variation in the concentrations of $H_2S_{(g)}$ in the magmatic gas from 0.001 to 3% only causes an expected increase in $H_2S_{(g)}$ and a very small decrease in $N_{2(g)}$ (Fig. 11a and b). In similar fashion, increasing the magmatic-gas concentrations of $HCl_{(g)}$ from 0.01 to 1% (not shown) and $HF_{(g)}$ from 0.01 to 0.2% (Fig. 11c and d) produces only the respective increases in $HCl_{(g)}$ and $HF_{(g)}$, although the concentration of $HCl_{(g)}$ in the resulting gas never reaches significant levels. Finally, increasing $\log fO_2$ in the magmatic gas from −13 to −5 induces a sharp drop in $H_2S_{(g)}$ by driving the following reaction:

$$H_2S_{(aq)} + 2O_{2(g)} \rightarrow HSO^-_{4(aq)} + H^+_{(aq)}, \quad (21)$$

to the right, which triggers a right-shift in reaction (17) with the consequent abrupt increase in $N_{2(g)}$ (Fig. 11e and f). Increasing $\log fO_2$ also produces a sharp drop in $H_{2(g)}$, but note that $H_{2(g)}$ concentrations are significant between $\log fO_2$ of −12.49 and −13 as low $HSO^-_{4(aq)}$ concentrations drive reaction (10) to the left. The large modeled increase in $\log fO_2$ also produces an increase in $SO_{2(g)}$, though it never reaches significant concentrations.

2.10. Case 7: effects of rock reaction

In case 7, we investigate the departure from case 1 caused by rock reaction. Starting with a mixture of 1 kg of ASW plus 0.1 kg of Merapi gas (1.1 kg total), we add between 0.001 and 100 g of volcanic rock into the mixture. We stop at 100 g of rock added (gra) because additions of more rock fail to influence the gas composition trends. Total enthalpy and pressure are fixed at case 1 values (for 0.1 kga), which produces a temperature range of 92.1–94.9°C. Note that rock addition causes only a small increase in mixture temperature as precipitating minerals consume gas species. The composition of the volcanic rock is the average composition (of 888 samples) of

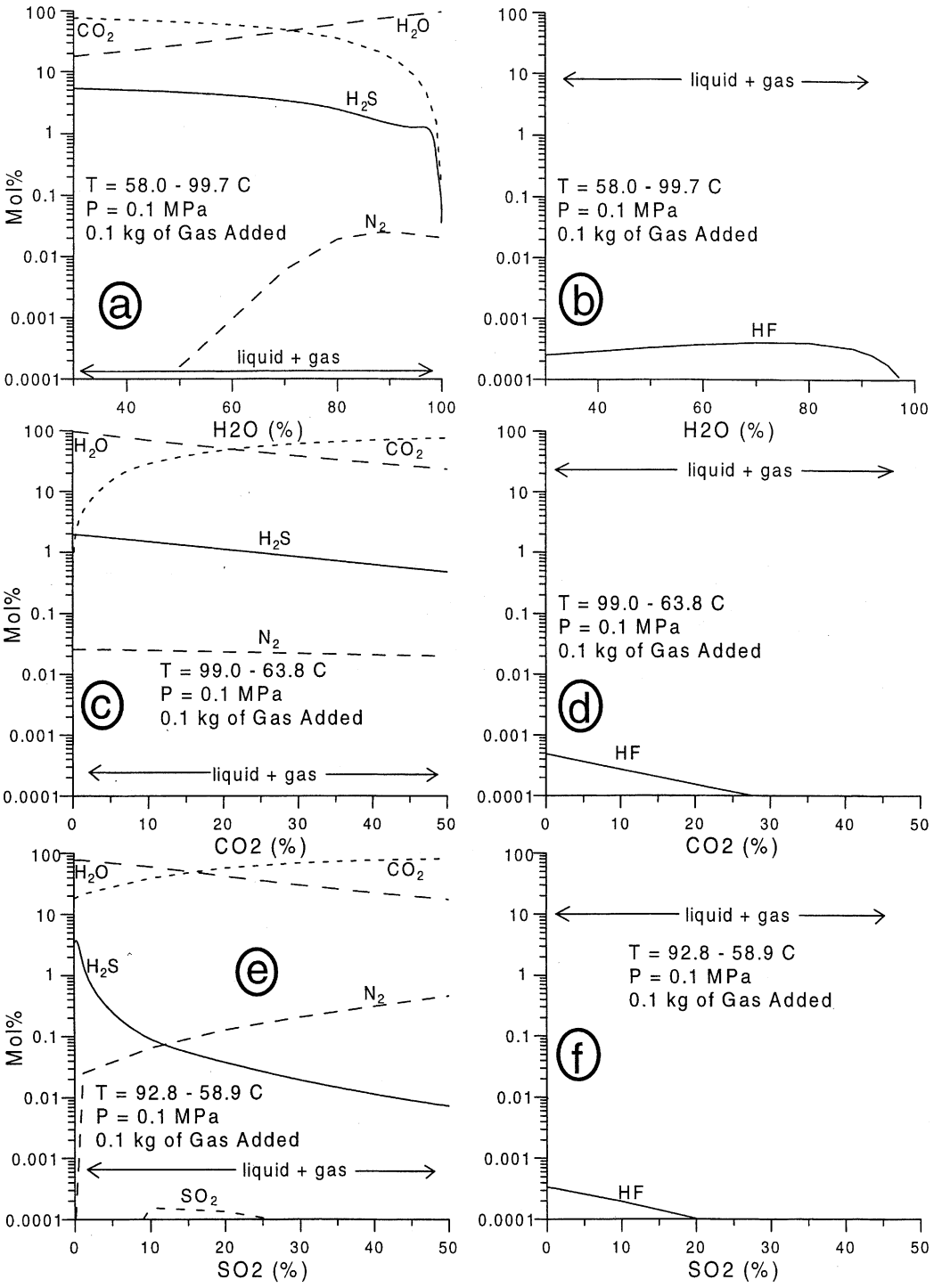

Fig. 10. Diagram showing mol% concentrations of the most abundant gas species of H, O, C, S, Cl, F, and N from reacting 1 kg of 25°C ASW with 0.1 kg of modified 915°C Merapi gas (gas/water = 0.1) containing variables amounts of: (a), (b) $H_2O_{(g)}$; (c), (d) $CO_{2(g)}$; and (e), (f) $SO_{2(g)}$ at 0.1 MPa (case 6, Fig. 2). Horizontal axes show the mol% of $H_2O_{(g)}$, $CO_{2(g)}$, and $SO_{2(g)}$, respectively, in the input magmatic gas. Temperature range applies as the calculations proceed from left to right on the diagrams.

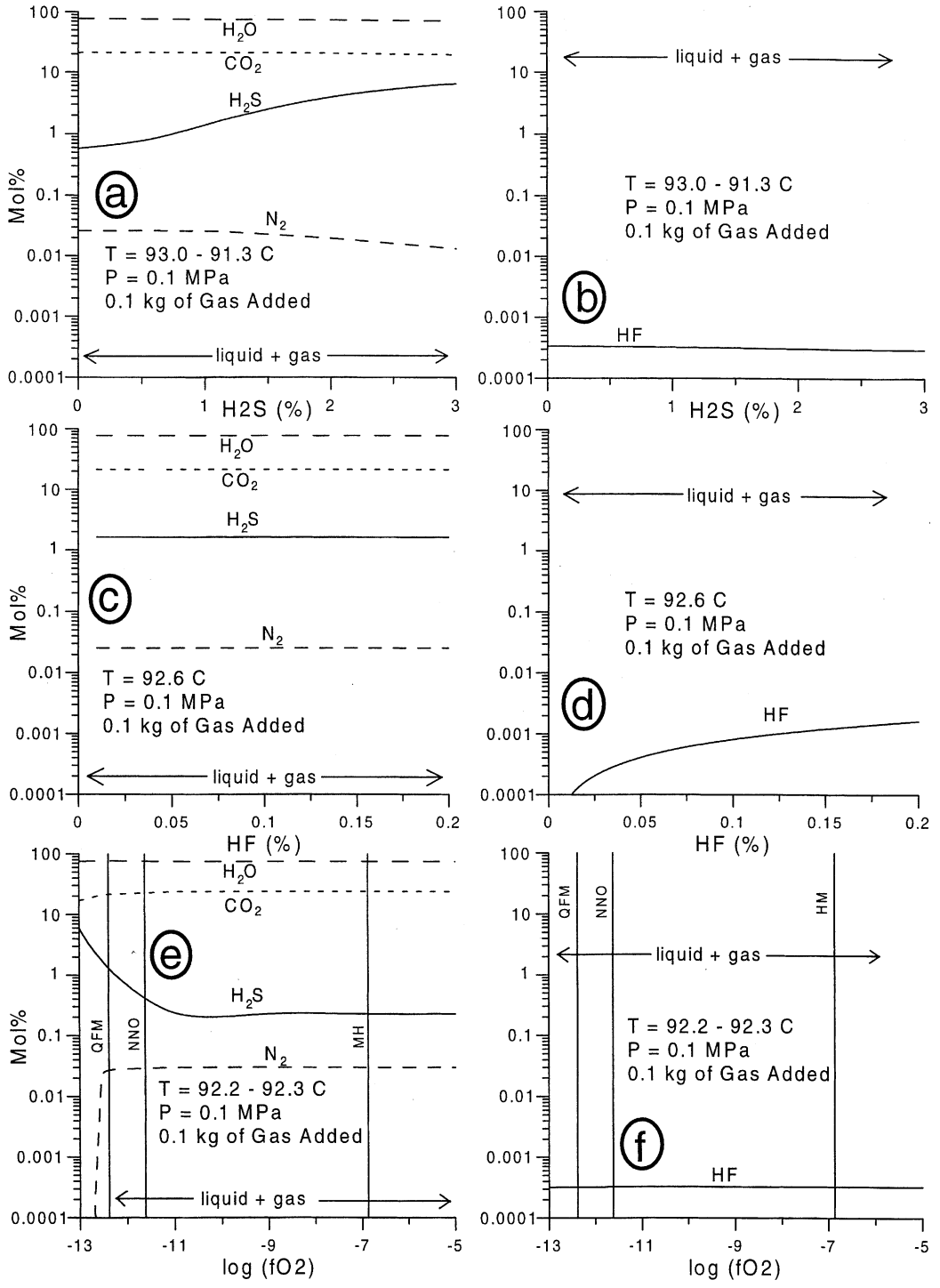

Fig. 11. Diagram showing mol% concentrations of the most abundant gas species of H, O, C, S, Cl, F, and N from the case 6 calculations (continued from Fig. 10) with variable amounts of: (a), (b) $H_2S_{(g)}$; (c), (d) $HF_{(g)}$; and (e), (f) $\log fO_{2(g)}$ in the input magmatic gas. Horizontal axes show the mol% of $H_2S_{(g)}$ and $HF_{(g)}$, and $\log fO_{2(g)}$, respectively, in the input magmatic gas. Temperature range applies as the calculations proceed from left to right on the diagrams.

medium-K acid andesites from Gill's (1981, p. 99) database of orogenic andesites. This composition represents a typical volcanic rock in convergent-plate settings. To model a wide range of volcanic rock compositions will require further investigation, but we think it likely that variations in rock composition would have little effect on the conclusion that rock reaction causes increases in $H_{2(g)}$, decreases in $H_2S_{(g)}$ and $HF_{(g)}$, and, if enough rock reacts, $CO_{2(g)}$ decrease also (see below).

Fig. 12a–f shows the resulting mineral assemblage, pH, molalities of aqueous F species, and gas composition over the course of the calculation. Rock reaction has a significant impact on $H_2S_{(g)}$ and $H_{2(g)}$. At between 0.3 and 11 gra, $H_2S_{(g)}$ increases due to the destruction of native sulfur caused by increasing pH (Fig. 12c) and the corresponding left-shift in reaction (16) and its $HSO^-_{4(aq)}$ equivalent. (Note the crossover between $HSO^-_{4(aq)}$ and $SO^{2-}_{4(aq)}$ at about 6 gra due to pH increase.) $H_{2(g)}$ also increases 10-fold between 0.3 and 11 gra as increasing concentrations of $H_2S_{(aq)}$ drive reaction (10) to the left though $H_{2(g)}$ never exceeds concentrations of 0.0001 mol%. At >11 gra, $H_2S_{(g)}$ decreases as it reacts substantially with ferrous iron in rock to form pyrite:

$$7H_2S_{(g)} + SO^{2-}_{4(aq)} + 2H^+_{(aq)} + 4FeO_{(rock)} \rightarrow 4FeS_{2(pyrite)} + 8H_2O_{(aq)}, \quad (22)$$

which is driven to the right by supply of $FeO_{(rock)}$. In contrast, $H_{2(g)}$ continues to increase sharply between 11 and 19 gra as pH climbs from 3.2 to 6.2, driving reaction (10) strongly to the left. But between 19 and 60 gra, $H_{2(g)}$ follows the decline in $H_2S_{(g)}$ (and $H_2S_{(aq)}$) from pyrite precipitation, which produces a consequent right-shift in reaction (10). At >60 gra both $H_2S_{(g)}$ and $H_{2(g)}$ increase once again owing to hematite precipitation:

$$SO^{2-}_{4(aq)} + 2H^+_{(aq)} + 8FeO_{(rock)} \rightarrow 4Fe_2O_{3(hematite)} + H_2S_{(g)}. \quad (23)$$

Rock addition also removes $HF_{(g)}$ owing to the production of Al fluoride complexes by the following reactions between >0.2 and 13 gra:

$$Al_2O_{3(rock)} + 2HF_{(g)} + 4H^+_{(aq)} \rightarrow 2AlF^{2+}_{(aq)} + 3H_2O_{(aq)}, \quad (24)$$

$$Al_2O_{3(rock)} + 4HF_{(g)} + 2H^+_{(aq)} \rightarrow 2AlF^{+}_{2(aq)} + 3H_2O_{(aq)}. \quad (25)$$

Reactions (24) and (25) are both driven by acid-destruction of rock under lower pH conditions. At >13 gra, as pH neutralizes, $HF_{(g)}$ is removed mostly by precipitation of fluorite between 14 and 49 gra:

$$2HF_{(g)} + CaO_{(rock)} \rightarrow CaF_{2(\,fluorite)} + H_2O_{(aq)}, \quad (26)$$

and, at >50 gra, by the precipitation of fluorapatite:

$$2HF_{(g)} + 10CaO_{(rock)} + 3P_2O_{5(rock)} \rightarrow 2Ca_5(PO_4)_3F_{(\,fluorapatite)} + H_2O_{(aq)}. \quad (27)$$

Precipitation of calcite at ≥19 gra consumes $CO_{2(g)}$ by the net reaction:

$$CO_{2(g)} + CaO_{(rock)} \rightarrow CaCO_{3(calcite)}, \quad (28)$$

whose intermediate steps (not shown) involving $HCO^-_{3(aq)}$ and $Ca^{2+}_{(aq)}$ are driven by rising pH (see Reed and Spycher, 1985, p. 253). Addition of significantly more than 100 g of rock severely depletes $CO_{2(g)}$, until the gas becomes virtually 100% $H_2O_{(g)}$ with minor amounts of $N_{2(g)}$.

Rock addition also consumes $SO_{2(g)}$ owing to precipitation of alunite between 1 and 14 gra:

$$3Al_2O_{3(rock)} + K_2O_{(rock)} + 4SO^{2-}_{4(aq)} + 2H_2O_{(aq)} + 8H^+_{(aq)} \rightarrow 2KAl_3(OH)_6(SO_4)_{2(alunite)}, \quad (29)$$

Fig. 12. Diagram showing the results from reacting andesite with a mixture of 0.1 kg of 915°C Merapi gas and 1 kg of 25°C ASW (gas/water = 0.1) at 0.1 MPa (case 7, Fig. 2). In this figure, we show the resulting: (a), (b) mineral assemblage; (c) pH; (d) molalities of the dominant aqueous species of F; and (e), (f) the mol% values of the major gas species of H, O, C, S, Cl, F, and N. The mineral phases include sulfur (S), alunite ($KAl_3(OH)_6(SO_4)_2$), calcite($CaCO_3$), muscovite ($KAl_2(AlSi_3O_{10})(OH)_2$), fluorite ($CaF_2$), rhodochrosite ($MnCO_3$), low albite ($NaAlSi_3O_8$), quartz ($SiO_2$), diaspore (AlO(OH), pyrite (FeS_2), anhydrite ($CaSO_4$), talc ($Mg_3Si_4O_{10}(OH)_2$), fluorapatite ($Ca_5(PO_4)_3F$), and hematite (Fe_2O_3). Horizontal axes show the g of andesite added to the mixture (water/rock ratio = 1100 g of mixture/g andesite added).

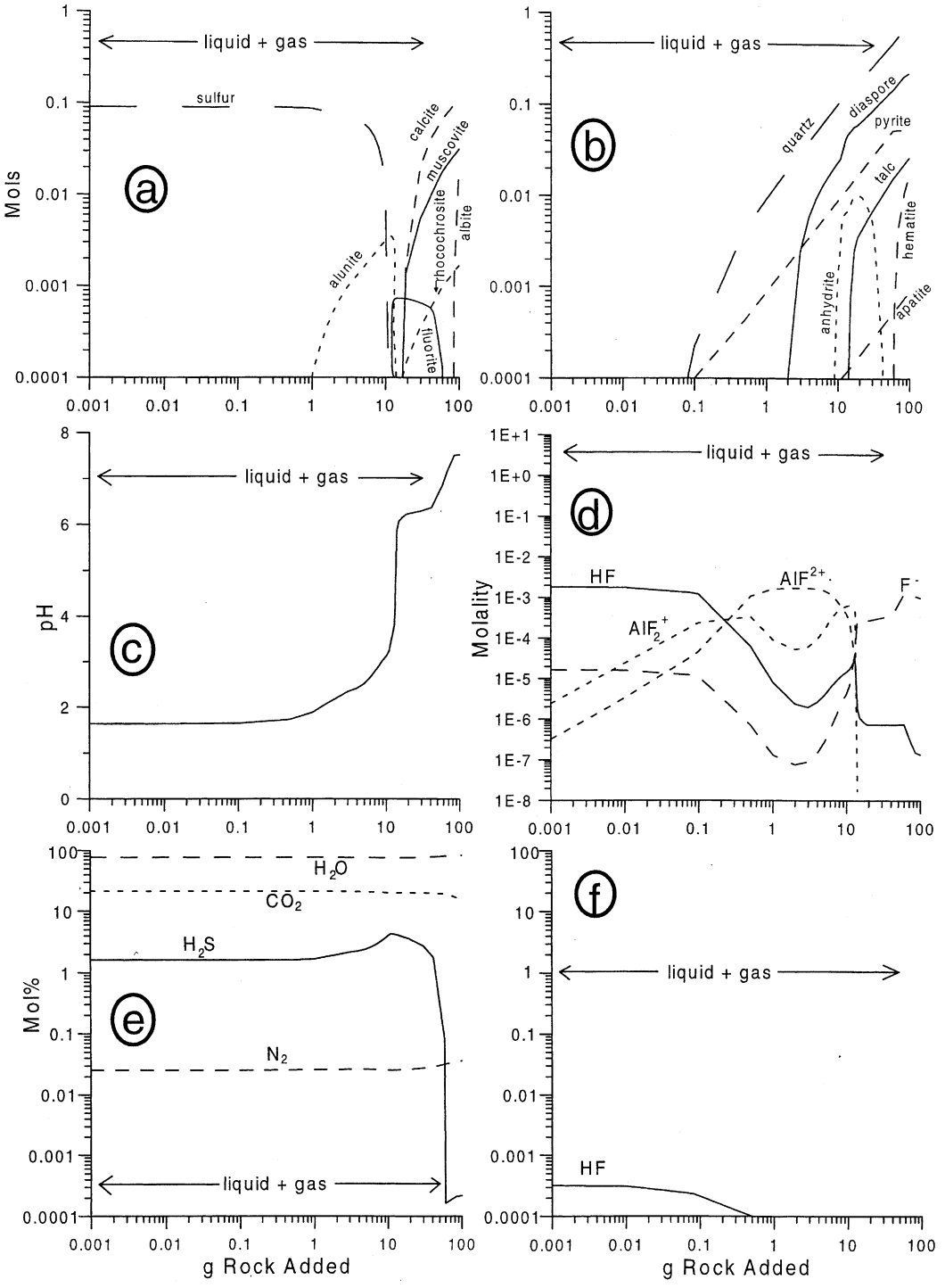
a
liquid + gas
sulfur
calcite
muscovite
albite
rhocochrosite
alunite
fluorite
Mols
b
quartz
diaspore
pyrite
talc
hematite
anhydrite
apatite
c
pH
d
HF
AlF^{2+}
AlF_2^+
F
Molality
e
H_2O
CO_2
H_2S
N_2
Mol%
f
HF
g Rock Added

Fig. 12.

and by the precipitation of anhydrite between 9 and 41 gra:

$$CaO_{(rock)} + SO_{4(aq)}^{2-} + 2H_{(aq)}^{+} \rightarrow CaSO_{4(anhydrite)} + H_2O_{(aq)}. \quad (30)$$

Precipitation of these sulfates consumes $SO_{4(aq)}^{2-}$ and drives reaction (4) to the right. Although insignificant amounts of $SO_{2(g)}$ exist throughout the case 7 calculations, there are some situations (e.g. case 3; case 5: mixing with acid sulfate waters) where it may be significant but rock reaction and simultaneous precipitation of sulfates might nevertheless seriously limit $SO_{2(g)}$ production.

Finally, rock injection devours $HCl_{(g)}$ by consuming $H_{(aq)}^{+}$ (Fig. 12c) and driving reaction (6) to the right. Again, while there are some situations (e.g. case 3; case 5: mixing with acid sulfate and neutral chloride waters) where $HCl_{(g)}$ may otherwise be significant, the pH increase caused by rock reaction might seriously limit its production.

The minerals that precipitate during the course of the calculations (Fig. 12a and b) form the predicted alteration assemblages for the reaction between acid sulfate–chloride fluids and andesite at relatively high water/rock ratios. The initial fluid is saturated with sulfur (Fig. 12a). As rock is added to the solution, the pH steps through a series of mineral buffer reactions as it increases from 1.64 to 7.52 (Fig. 12c). As pH rises, the sequence of overlapping minerals assemblages that form are as follows (minerals listed in order of precipitation in each group): (1) intense advanced argillic at pH 1.64–1.89 (sulfur–quartz–pyrite); (2) advanced argillic at pH = 1.89–3.82 (sulfur–quartz–pyrite–alunite–diaspore–anhydrite–apatite–fluorite); (3) sericitic at pH = 3.82–7.51 (quartz–pyrite–alunite–diaspore–anhydrite–apatite–fluorite–talc–muscovite–calcite–rhodochrosite–hematite); and (4) propylitic at pH = 7.51–7.52 (quartz–pyrite–diaspore–apatite–talc–muscovite–calcite–rhodochrosite–hematite–albite).

2.11. Discussion of modeling results

The modeling demonstrates, with a few important exceptions, that the effects identified in case 1 are unchanged even with wide variations in the input parameters (cases 2–7). So we discuss the case 1 results first and then address significant modifications encountered in cases 2–7. Case 1 shows that as the g/w ratio increases from 0.0002 to <0.008, the solution heats up slowly, pH decreases, and all gases either dissolve into the aqueous phase or, at g/w ratios >0.0008, precipitate as sulfur. At g/w ratios of >0.002, sulfur precipitation scrubs more $SO_{2(g)}$ and $H_2S_{(g)}$ than hydrolysis. Studies of crater lake waters demonstrate that temperature increases, pH decreases, and sulfur precipitates when magmatic gas discharges into volcanic crater lakes (Brantley et al., 1987; Rowe et al., 1992; Rowe, 1994; Campita et al., 1996). Sulfur also derives from disproportionation of $SO_{2(g)}$ in acid–sulfate epithermal systems (Reyes, 1991).

Hence, the calculations predict that for g/w < 0.008, such as when degassing magma intrudes a very wet volcanic edifice, scrubbing will eradicate all gas precursors including gases with low solubilities in water, like $CO_{2(g)}$. For example, McGee and Gerlach (1998) have observed a sharp decrease in cold magmatic $CO_{2(g)}$ emissions from soil at Mammoth Mountain at the time of spring snow melt.

As the g/w ratio increases from 0.008 to 1.7, temperature increases significantly, pH decreases more drastically, and less soluble gases ($CO_{2(g)}$, $H_2O_{(g)}$, $H_2S_{(g)}$, $N_{2(g)}$) exsolve from the aqueous phase. Proceeding across the liquid-plus-gas region, the predicted gases evolve from $CO_{2(g)}$–$H_2O_{(g)}$–$H_2S_{(g)}$–$N_{2(g)}$ ($T \leq 81°C$; g/w ≤ 0.07)) to $H_2O_{(g)}$–$CO_{2(g)}$–$H_2S_{(g)}$ ($T = 81$ to ~106°C; g/w = 0.07–1.8). Minor amounts (>0.0001 mol%) of $HF_{(g)}$ and $HCl_{(g)}$ form at 0.06 and 0.2 kga, respectively; continuing across the liquid-plus-gas region, $HF_{(g)}$ increases loglinearly approaching near-magmatic levels when the mixture reaches the gas-only region; in contrast, $HCl_{(g)}$ increases at an accelerating rate as pH drops to <1 (g/w > 0.4), reflecting the low solubility of $HCl_{(g)}$ in very acidic solutions, and it also reaches near-magmatic levels upon reaching the gas-only region. The predicted $CO_{2(g)}$–$H_2O_{(g)}$–$H_2S_{(g)}$–$N_{2(g)}$ gases at g/w ≤ 0.07 contain much more $H_2S_{(g)}$ than most cold volcanic $CO_{2(g)}$-rich discharges (e.g. the cold $CO_{2(g)}$, emissions from Mammoth Mountain; Farrar et al., 1995), suggesting that cold volcanic discharges generally derive from magmatic gases that have reacted with water, removing acid gases, and with rock, removing $H_2S_{(g)}$ (see below). In contrast, the

$H_2O_{(g)}$–$CO_{2(g)}$–$H_2S_{(g)}$ gases at g/w = 0.07–1.8 are a reasonable match to hydrothermal gas discharges from volcanoes. For example, hydrothermal discharges from boiling-point and superheated fumaroles from Cascade-Range and Aleutian-Arc volcanoes are dominated by $H_2O_{(g)}$, $CO_{2(g)}$, and $H_2S_{(g)}$; their chemical compositions, along with isotopic evidence for magmatic sources for C and He, suggest that these gases contain a magmatic component that is heavily modified from scrubbing by deep hydrothermal (150–350°C) and shallow meteoric water (Symonds et al., 2001).

Over most of the liquid-plus-gas region, the predicted gas precursors are elevated concentrations of $CO_{2(g)}$ and $H_2S_{(g)}$, small concentrations of $HF_{(g)}$ (increasing with the amount of gas added) with $HF_{(g)} \gg HCl_{(g)}$, and minute concentrations of $SO_{2(g)}$ and $HCl_{(g)}$, assuming as in case 1, that rock reaction is absent. However, the predicted amounts of $HF_{(g)}$ are difficult to detect in gas samples and may be diminished by rock reaction. Just before entering the gas-only region, significant amounts of $HCl_{(g)}$ exsolve from the residual very acidic solution.

When enough hot magmatic gas is added to water (g/w > 1.7), the mixture enters the gas-only region, producing a large increase in the relative $SO_{2(g)}$ concentration. Addition of more magmatic gas increases the temperature and magmatic-gas fraction of the gas discharges. During this stage, the gas discharges are essentially mixtures of magmatic gas and steam as observed in 600–830°C fumaroles at Mount St. Helens between 1980 and 1982 (Gerlach and Casadevall, 1986). Finally, a pathway dries out sufficiently to allow pure magmatic gases to vent to the atmosphere.

The case 1 calculations suggest that $CO_{2(g)}$ and $H_2S_{(g)}$ are the main species to monitor over much of the liquid-plus-gas region. $HF_{(g)}$ is also possible, but it is likely to be trivial and highly variable because of its high solubility in magma and reaction of the mixture with rock (case 7) can diminish drastically $HF_{(g)}$ concentrations by forming Al fluoride complexes or precipitation of F-bearing minerals (e.g. fluorite, and fluorapatite). Rock reaction can also strongly degrade $H_2S_{(g)}$ concentrations by forcing pyrite precipitation. Hence, if magmatic gas reacts with both water and significant amounts of rock, $CO_{2(g)}$ may be the only anhydrous species emitted in sufficient abundance to monitor, although if the gas–water mixture reacts extensively with rock, $CO_{2(g)}$ can also be consumed by precipitation of calcite.

$H_{2(g)}$ may also be a poor choice for monitoring because it can be affected by several processes. The case 1 calculations suggest that magmatic $H_{2(g)}$ may be scrubbed by aqueous sulfur redox equilibria; reduction of $SO^{2-}_{4(aq)}$ to $H_2S_{(aq)}$ by reaction (10) consumes all available $H_{2(g)}$. Cases 2–7 show that $H_{2(g)}$ concentration is also influenced by temperature, the compositions of the aqueous phase (pH, activities of $SO^{2-}_{4(aq)}$ and $H_2S_{(aq)}$), the fO_2 of the magmatic gas, and the extent of rock reaction. Thus, there are several hydrothermal processes that may affect $H_{2(g)}$ concentration. On the other hand, there may be some systems where $H_{2(g)}$ survives passage through hydrothermal waters and would be a useful indicator of magmatic input. Thermochemical modeling of the geothermal gases from the Fushime geothermal system in Japan suggests that the kinetics of $H_{2(g)}$ reactions with $SO^{2-}_{4(aq)}$ and $H_2S_{(aq)}$ are too slow to influence $H_{2(g)}$ concentrations at Fushime (Akaku et al., 1991). Nonetheless, we think that in general it will be difficult to interpret changes in $H_{2(g)}$ emissions as a clear indicator of magmatic unrest.

The case 1 calculations also suggest that hydrolysis and sulfur precipitation reactions prevent significant $SO_{2(g)}$ and $HCl_{(g)}$ emissions from wet low-temperature systems; only nearly dry or very acidic (for $HCl_{(g)}$), and higher temperature systems will vent significant quantities of these gases. The calculations in cases 2–7 confirm that superheated dry pathways greatly facilitate transport of $SO_{2(g)}$ and $HCl_{(g)}$ from magma to the atmosphere. Moreover, heating of wet pathways by conduction will decrease the amount of gas necessary to complete the dry-out process, as shown in case 4. Cases 2–7 also demonstrate the difficulty of obtaining large $SO_{2(g)}$ (especially $SO_{2(g)} > H_2S_{(g)}$) or $HCl_{(g)}$ emissions from within the liquid-plus-gas region. The only mechanisms in cases 1–7 that produce significant $SO_{2(g)}$ and $HCl_{(g)}$ within the liquid-plus-gas region are as follows (in decreasing order of effectiveness): (1) elevated pressure (case 3); (2) acidification of the liquid phase, especially for $HCl_{(g)}$ if pH < 0.5 (cases 1 and 5); and (3) increasing the activities of $SO^{2-}_{4(aq)}$ (for $SO_{2(g)}$) and $Cl^{-}_{(aq)}$ (for $HCl_{(g)}$) in the liquid phase (case 5). Note that, although gas solubility generally increases with pressure, the temperature

range of the liquid-plus-gas region shifts to higher temperature with increasing pressure, lowering the solubilities of $SO_{2(g)}$ and $HCl_{(g)}$ in solution and volatilizing $SO_{2(g)}$ from elemental sulfur.

How much $SO_{2(g)}$ and $HCl_{(g)}$ can realistically degas from hydrothermal solutions via mechanisms (1)–(3)? Rowe et al. (1992) found evidence for significant $HCl_{(g)}$ but little $SO_{2(g)}$ release from the extremely acidic, sulfate–chloride crater lake at Poás ($T = 44$–$87°C$, pH = 0.2 to −0.6, $SO^{2-}_{4(aq)}$ = up to 286,000 mg/kg, $Cl^{-}_{(aq)}$ = up to 129,000 mg/kg). This confirms that $HCl_{(g)}$ readily exsolves from hot hyperacidic liquids, but also demonstrates that, even in these extreme brines, much higher temperatures — and therefore pressures — are apparently essential to exsolve significant $SO_{2(g)}$. Thus, effective $SO_{2(g)}$ exsolution from hydrothermal solutions requires all three mechanisms.

However, we expect that such hot, high-pressure, acid sulfate fluids will have short residence times before they react with host rock to dissolve rock-forming cations (e.g., Na and K) and increase pH. Many studies have shown that hydrothermal solutions react with their host rocks and form alteration assemblages consistent with fluid-mineral equilibrium at pH = 3–7 (Brimhall and Ghiorso, 1983; Reed and Spycher, 1984; Giggenbach, 1988). Reaction with wall rocks is also consistent with less acidic (pH = 3–4) sulfate-rich fluids sampled at volcanic geothermal systems such as Bacon-Manito, Palinpinion, Pinatubo, and Tongonan (Reyes, 1990; Delfin et al., 1992). Equilibration between silicate minerals and fluids in hydrothermal systems is apparently on the timescale of weeks to months (Reed, 1997); hence, partial fluid-rock reaction with concomitant pH increase can occur relatively rapidly.

Rock reaction (case 7) limits $SO_{2(g)}$ and $HCl_{(g)}$ degassing by precipitating sulfates and increasing pH, respectively. Even flash vaporization of rock-reacted sulfate-rich hydrothermal fluids to superheated vapor fails to produce $SO_{2(g)}$, owing to precipitation of sulfates (Gerlach et al., 1996). Therefore, we expect that long-resident hydrothermal solutions that have reacted with their host rocks will contain enough dissolved cations and lack sufficiently low pH conditions to degas much, if any, $SO_{2(g)}$ and $HCl_{(g)}$, even if they have high temperatures and high sulfate concentrations. But if magmatic gases are discharged into a higher pressure hydrothermal system at a rate that spawns hydrogen ions faster than water–rock reactions can consume them, it may be possible to produce a transient condition of low pH, high temperature, and high sulfate that generates hydrothermal $SO_{2(g)}$ and $HCl_{(g)}$. Indeed, Christenson (2000) argues that this type of transient condition aided $SO_{2(g)}$ production from stored hydrothermal sulfur during the 1995–1996 eruptions of Mount Ruapehu. But, in general, we expect that significant $SO_{2(g)}$ degassing from hydrothermal solutions is relatively rare. In contrast, $HCl_{(g)}$ degassing may occur during the dry-out of near-surface acidic hydrothermal fluids as well as from the rare conditions that promote $SO_{2(g)}$ degassing from deeper hydrothermal solutions.

The obvious way to monitor the dry-out process is to measure concentrations or emission rates of species with both large and small solubilities in water. $CO_{2(g)}$ and $H_2S_{(g)}$, in that order, are valuable for their small water solubilities, although $H_2S_{(g)}$ can be consumed by rock reaction. In contrast, $SO_{2(g)}$ and $HCl_{(g)}$ have large water solubilities, except for $HCl_{(g)}$ in low pH solutions, and are useful indicators of a dry pathway. Finally, the modeling suggests that the $H_2O_{(g)}/CO_{2(g)}$, $SO_{2(g)}/CO_{2(g)}$, $CO_{2(g)}/HCl_{(g)}$, $SO_{2(g)}/H_2S_{(g)}$, $H_2S_{(g)}/CO_{2(g)}$, and possibly $HCl_{(g)}/HF_{(g)}$ ratios might help monitor drying out of wet pathways; owing to the potentially different solubilities of $HCl_{(g)}$ and $SO_{2(g)}$ in shallow low pH solutions, $HCl_{(g)}/SO_{2(g)}$ might be useful in monitoring the drying out of a shallow acidic hydrothermal system.

Besides the obvious implications for volcano monitoring, scrubbing also produces acidic fluids that dissolve and hydrothermally alter competent volcanic rock, processes that are closely linked to the generation of volcanic landslides and debris flows (López and Williams, 1993; Crowley and Zimbelman, 1997). The results of case 7 and other modeling studies (Reed, 1992, 1997; Christenson and Wood, 1993) demonstrate that hydrothermal fluids, acidified with magmatic $SO_{2(g)}$ and $HCl_{(g)}$, can dissolve and alter fresh volcanic rock; the modeling also reproduces the alteration assemblages (argillic, sericitic, propylitic) observed at many terrestrial volcanoes. Rock dissolution and hydrothermal alteration can enhance the odds of landslides by weakening the overall edifice and producing instability along fault planes,

dikes, bedding surfaces, and other structures (López and Williams, 1993; Crowley and Zimbelman, 1997). If a sector of altered rock fails, clay-size minerals in the alteration also can contribute to the formation of debris flows that can travel farther as a cohesive unit than more granular flows (Scott et al., 1995). The rates of hydrothermal alteration at active volcanoes are poorly understood. One of the best assessments is from Nevado del Ruiz where López and Williams (1993) estimate rates of alteration to be 12,600 m^3 of rock per year along a major fault zone. They suggest that these rates can produce sufficient alteration to generate landslides in a few thousand years, at least at some volcanoes.

3. Scrubbing case studies

We use emission rate data from eruptions at Crater Peak on Mount Spurr (1992), Mount St. Helens (1980), Mount Pinatubo (1991), and the ongoing eruption of Popocatépetl to illustrate the broad range of impacts that scrubbing can have on volcano degassing. We feel strongly that these case studies are best interpreted in the light of scrubbing processes. Nonetheless, we acknowledge that other hypotheses could account for these observations, despite their consistency with scrubbing or its absence. Furthermore, we emphasize that scrubbing is only one process that affects volcanic degassing and that other factors (e.g., magmatic volatile solubility, magma convection, sealing of gas-transport permeability by hydrothermal alteration, plugging by shallow intrusions, or dome emplacement, and mineral precipitation reactions) also influence the emission rates and compositions of discharged volatiles.

We specifically focus on using the extensive parameter, emission rate, to illustrate scrubbing because this is the type of gas data most commonly collected during an eruptive cycle. Nonetheless, we acknowledge that the model calculations are best suited to explain intensive parameters such as the compositions of low-temperature fumarolic gases (Symonds et al., 2001). The models effectively represent the degree and magnitude of scrubbing along only a single pathway of a volcanic system. However, a volcanic system impacted by scrubbing may have a range of wet to dry pathways and thus a measurable $SO_{2(g)}$ emission rate even though the modeling predicts that scrubbing would capture virtually all $SO_{2(g)}$ along the wet pathway.

The case studies begin with the Crater Peak eruption, a documented example (Doukas and Gerlach, 1995) where scrubbing so dramatically shut down nonexplosive $SO_{2(g)}$ emissions that it became, for us, an archetype that motivated the present study. At the other extreme is Popocatépetl where scrubbing has had only minor effect on degassing. All emission rates are in metric tons per day (t/d, 1 metric ton $= 10^3$ kg).

3.1. Crater peak

We summarize background material for Crater Peak and its 1992 eruptions from Keith (1995). Crater Peak is a satellite basaltic andesite stratovolcano on the south side of the Mount Spurr volcanic complex, a Quaternary sequence of calc-alkaline andesites west of Cook Inlet and Anchorage, Alaska. Glaciers fill Spurr caldera to 0.5 km depths and surround Crater Peak on all but its south side. Deep snow covers Crater Peak during winter. Crater Peak lies on the projected extension from a regional fault to the east that may permit infiltration of meteoric waters derived from melted snow and ice to sustain a hydrothermal system under the volcano. Springs along a 1 km-long zone release warm water at the southern base of Crater Peak, and a lake was present in its crater ever since the previous eruption in 1953. Seismic data suggest that magma intruded at 5–15 km depth in August 1991 and then migrated to shallower depths of 1–2 km before the first of three basaltic andesite eruptions on 27 June, 18 August and 17 September 1992. A period of extremely intense seismicity, presumably related to shallow intrusion, occurred on 9 November 1992. What follows is a summary of the evidence for scrubbing of acid gases prior to, during, and after the eruptions (Doukas and Gerlach, 1995). The evidence is based largely on airborne COSPEC and MIRAN (an infrared spectrophotometer by Foxboro Analytics) data for $SO_{2(g)}$ and $CO_{2(g)}$ emissions, respectively.

The first COSPEC measurements during the period of precursory seismicity in August 1991 showed $SO_{2(g)}$ column abundance (ppm m) at the volcano was indistinguishable from background and from baseline data obtained on 22 July 1991 (Fig. 13a).

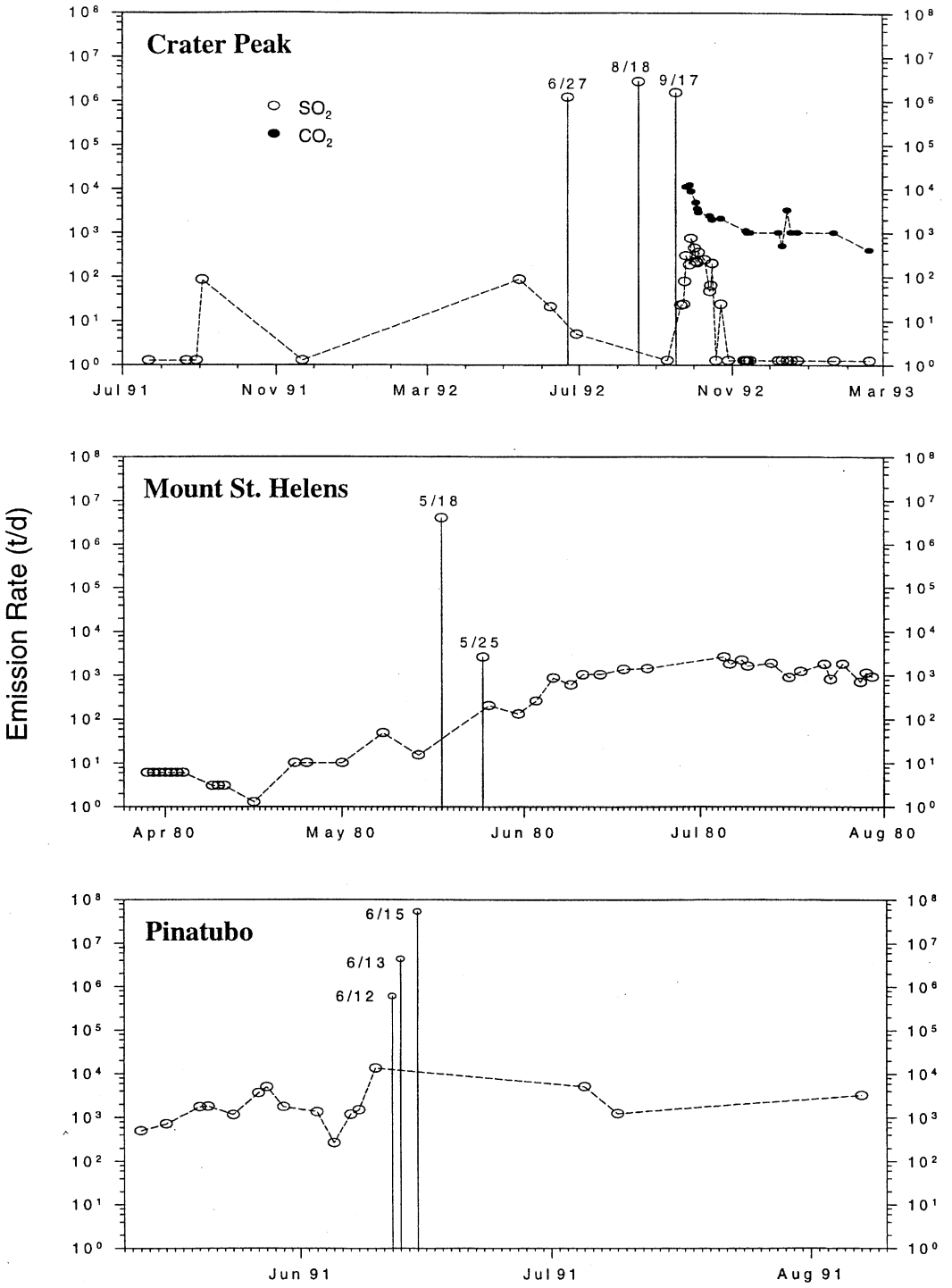
Crater Peak
SO2
CO2
6/27
8/18
9/17
Jul 91
Nov 91
Mar 92
Jul 92
Nov 92
Mar 93
Mount St. Helens
5/18
5/25
Apr 80
May 80
Jun 80
Jul 80
Aug 80
Pinatubo
6/15
6/13
6/12
Jun 91
Jul 91
Aug 91
Emission Rate (t/d)

Fig. 13.

Indeed, all COSPEC measurements from 22 July 1991 to 24 September 1992 — seven days after the last eruption — indicated only background to minor noneruptive $SO_{2(g)}$ emissions of <100 t/d (Fig. 13a). Two measurements in May and June 1992 during the periods of increased seismicity gave only 88 and 21 t/d, respectively. COSPEC measurements on 29 June, just two days after the first eruption, showed $SO_{2(g)}$ emission rates of only 5 t/d. Measurements on 10 September, a week prior to the 17 September eruption, were at background levels; measurements in the week following this eruption on 21, 23, and 24 September were only slightly above background (23, 24, and 79 t/d, respectively). These results are striking for a period of time that included: (a) the onset of precursory seismicity beneath Crater Peak (August 1991); (b) the peaking in frequency of volcanotectonic earthquakes and the initiation of volcanic tremor bursts (5 June 1992); and (c) three explosive eruptions that released $SO_{2(g)}$ at high rates of 1200 kt/d (27 June 1992), 2700 kt/d (18 August 1992), and 1500 kt/d (17 September 1992) (Fig. 13a). The $SO_{2(g)}$ emission rates for explosive eruptions reported here and below are calculated from the total $SO_{2(g)}$ output (Bluth et al., 1995) divided by the duration of the event (Eichelberger et al., 1995).

$SO_{2(g)}$ emissions from a volcano depend on the net sum of $SO_{2(g)}$ supplied by magma degassing and $SO_{2(g)}$ removed by scrubbing; the dominant process will have to be evaluated case by case. Gardner et al. (1998) argue that very low intereruptive $SO_{2(g)}$ emissions between 27 June and 17 September 1992 reflect the near absence of intereruptive magmatic degassing during this period. But based on the above evidence, changes in crater lake water (see below), persistently strong $H_2S_{(g)}$ odors (see below), and analogies with volcanoes that release significant $SO_{2(g)}$ during precursory and intereruptive stages (e.g. Pinatubo and Popocatépetl; see below), significant magmatic degassing (e.g. at least several hundred t/d of $SO_{2(g)}$) seems likely throughout the eruptive sequence. Thus, the puzzling record of low $SO_{2(g)}$ emissions at Crater Peak led to the speculation that scrubbing by subvolcanic groundwater effectively masked noneruptive emissions of $SO_{2(g)}$.

Given a sufficiently permeable edifice, the presence of subvolcanic groundwater was presumed highly likely because of the abundant surface sources of melt water that could rapidly recharge subvolcanic reservoirs during the summer and fall months of the eruptions. Hot springs at the base of the volcano, with temperatures of 40.2°C and 477 ppm $SO^{2-}_{4(aq)}$ in 1985 (Motyka and Nye, 1993), supported the premise. Scrubbing of $SO_{2(g)}$ would also explain the fourfold increase in the $SO^{2-}_{4(aq)}$ content of the Crater Peak lake water prior to the first eruption (Keith et al., 1995). The persistently strong and nauseating $H_2S_{(g)}$ odor endured regularly during airborne monitoring flights, despite only minor to background $SO_{2(g)}$, could also be explained by $SO_{2(g)}$ scrubbing. Large $SO_{2(g)}$ emissions observed by satellite-based TOMS (Bluth et al., 1995) were nevertheless possible during explosive eruptions because $SO_{2(g)}$ in magma ascending rapidly to the surface was degassed directly to the atmosphere, free of interactions with liquid water. Interestingly, the TOMS data also indicated that 15–25% of the sulfur released during the three eruptions was in the form of $H_2S_{(g)}$. Since $H_2S_{(aq)}$ is a product of $SO_{2(g)}$

Fig. 13. $SO_{2(g)}$ (open ovals) and $CO_{2(g)}$ (filled ovals) time series emission rate data for eruptions at: (a) Crater Peak (1992); (b) Mount St. Helens (1980); and (c) Pinatubo (1991). Emission rates are in metric tons per day (t/d, 1 metric ton = 10^3 kg). Except for Crater Peak, the time series axes are scaled in months (major interval) and days (minor interval); both major and minor intervals are in months for Crater Peak. Dashed lines connect $SO_{2(g)}$ and $CO_{2(g)}$ emission rates based on COSPEC and MIRAN data for noneruptive degassing. Note that $CO_{2(g)}$ measurements at Crater Peak did not begin until 25 September 1992. Solid drop lines connect $SO_{2(g)}$ emission rates for explosive degassing to the time series axes at the indicated dates; these rates are calculated from TOMS-based $SO_{2(g)}$ output and duration of explosive events, except for the 5/25 event at Mount St. Helens, which is based on COSPEC data obtained in the waning stages of an explosive eruption. The sources of COSPEC, MIRAN, TOMS, and eruption duration data are as follows: Crater Peak (Bluth et al., 1995; Doukas and Gerlach, 1995; Eichelberger et al., 1995); Mount St. Helens (Stoiber et al., 1980; Casadevall et al., 1981; Gerlach and McGee, 1994; McGee and Casadevall, 1994); Pinatubo (Bluth et al., 1992; Daag et al., 1996; Wolfe and Hoblitt, 1996). Reports of 'background' or 'zero' COSPEC-based $SO_{2(g)}$ emission rates at Crater Peak and Mount St. Helens are represented by points tangent to the time series axes, since zero cannot be represented on the log scale. The report of '3–10 t/d' for the first seven days of measurements (29 March to 4 April) at Mount St. Helens (Casadevall et al., 1981), is represented by a median value of 6 t/d for these dates. $SO_{2(g)}$ emission data are lacking for explosive eruptions at Mount St. Helens on 12 June and 22 July 1980. Note the trend of logarithmically increasing $SO_{2(g)}$ emission rates at Mount Pinatubo from 7–8 June to 15 June 1991.

hydrolysis (reactions (4) and (5)), a related conjecture was that sulfur degassed noneruptively as $SO_{2(g)}$ and converted to $H_2S_{(aq)}$ could be released later as $H_2S_{(g)}$ during boiling caused by heating from ascending and explosively erupting magma. To test the scrubbing hypothesis, the MIRAN instrument used for measuring $CO_{2(g)}$ emissions at Mount St. Helens in 1980–1981 (Harris et al., 1981) was shipped on 23 September to the Alaska Volcano Observatory. The expectation was that compared to $SO_{2(g)}$, $CO_{2(g)}$ emissions would be affected appreciably less by scrubbing.

On 25 September, eight days after the 17 September eruption, $SO_{2(g)}$ emissions reached 300 t/d (Fig. 13a). At the same time, the first MIRAN measurements showed $CO_{2(g)}$ emissions of 11 kt/d (Fig. 13a). Doukas and Gerlach (1995) suggest that by this time heat supplied from shallow magma emplaced during the last eruption had temporarily dried out a vapor-dominated pathway to the surface, thus diminishing $SO_{2(g)}$ scrubbing. $SO_{2(g)}$ emission rates peaked near the end of September at 750 t/d, coincident with a $CO_{2(g)}$ emission rate of 9 kt/d, only about one week after the dry-out zone was established. By early October, removal of heat by recharge of meteoric water apparently began to outpace the supply of heat from magma and hot rock. The dry escape route through the wet edifice began to close. $SO_{2(g)}$ emissions dropped below 450 t/d while $CO_{2(g)}$ emissions remained at 2–5 kt/d. After mid-October, the system became effectively water saturated and $SO_{2(g)}$ emissions fell to background levels and stayed there, even after the intense earthquake swarms on 9 November, although strong $H_2S_{(g)}$ odors were evident during airborne monitoring flights. $CO_{2(g)}$ emissions remained near 1 kt/d and stayed at this level until January 1993. Occasional later measurements showed lower $CO_{2(g)}$ levels of only a few hundred tons per day.

Taken together, the $CO_{2(g)}$ and $SO_{2(g)}$ emissions from 25 September to about 15 October 1992, indicate that magma was degassing through boiling water as well as through a zone of dry rock. Molar ratios of $CO_{2(g)}/SO_{2(g)}$ for magmatic gases from convergent-plate volcanic systems are usually in the range of 1–10 (Williams et al., 1992; Symonds et al., 1994). The models discussed above predict much higher $CO_{2(g)}/SO_{2(g)}$ ratios if a significant part of the degassing takes place through boiling water. During the 25 September–15 October period, most of the molar $CO_{2(g)}/SO_{2(g)}$ values at Crater Peak are >20, but they are not >100 as might be expected if dry pathways for degassing were absent (Doukas and Gerlach, 1995). For example, the $CO_{2(g)}$ emission rates of 11 and 12 kt/d and the corresponding $SO_{2(g)}$ emissions of 300–190 t/d give molar $CO_{2(g)}/SO_{2(g)}$ ratios of 53 and 92 on 25 and 28 September, respectively. These results suggest that much of the magmatic gas was scrubbed by water during the week after the 17 September eruption, when on 21, 23, and 24 September, $SO_{2(g)}$ emissions were, respectively, only 23, 24, and 79 t/d. $CO_{2(g)}$ emissions of 1–3 kt/d after mid-October suggest that either boiling continued to release aqueous $CO_{2(g)}$ (and presumably $H_2S_{(g)}$) or emplaced magma continued to degas. $CO_{2(g)}$ emissions continued after the 9 November earthquake swarms, which we speculate were related to intrusions too small to penetrate or dry out the water-saturated system and release $SO_{2(g)}$ but large enough to cause boiling and release $CO_{2(g)}$ and $H_2S_{(g)}$ from the aqueous phase.

Integrating the noneruptive $SO_{2(g)}$ emission rate data from 25 September 1992 to 18 February 1993 gives a total of only $\sim$6 kt. This is small compared to the 800 kt of $SO_{2(g)}$ released in noneruptive emissions from the 1989–1990 eruptions of nearby Redoubt Volcano (Casadevall et al., 1994), even though both recent eruptive sequences at Redoubt (Gardner et al., 1994; Scott and McGimsey, 1994; Miller, 1994) and Crater Peak (Eichelberger et al., 1995) involved similar amounts of andesitic magma.

3.2. Mount St. Helens

Compared to Crater Peak 1992, where scrubbing was likely important throughout most of the eruptive cycle, Mount St. Helens 1980 is an example where scrubbing was likely significant only in the early part of the eruptive cycle (Fig. 13b). Measurements of sulfur dioxide emission rates commenced on 29 March 1980 and continued on a regular basis until September 1988 (Stoiber et al., 1980, 1981; Casadevall et al., 1981; McGee and Casadevall, 1994). Prior to the 18 May 1980 climactic explosion, there was a 52-day period of phreatic eruptions and nonexplosive degassing that began on 27 March. The $SO_{2(g)}$ emission rates were very low (<50 t/d) at this time, a result that was emphasized as somewhat

unexpected by Stoiber et al. (1980, 1981). The highest of the 16 emission rates determined prior to 18 May was 48 t/d; the second highest was 15 t/d; the remaining 14 were 10 t/d or less. Although the 18 May eruption released $SO_{2(g)}$ at a rate of 4000 kt/d (Fig. 13b), emission rates just 4 days before were only 15 t/d. Noneruptive emission rates increased after the 18 May eruption and the second explosive eruption on 25 May but still remained relatively low (130–260 t/d) until at least 3 June (Fig. 13b). Emissions on 6 June jumped to 860 t/d and were sustained at high levels for several months thereafter (Fig. 13b) — finally reaching levels comparable to emission rates that had been observed at other actively erupting volcanoes, mostly in Central America (Stoiber et al., 1980, 1981). Thus, low emission rates were common for at least 50 days before and about 20 days after the paroxysmal eruption of 18 May.

Absorption of magmatic $SO_{2(g)}$ emissions by a hydrothermal system was mentioned as a possible cause of the peculiarly low $SO_{2(g)}$ emission rates, but never given further consideration (Casadevall et al., 1981). Instead, the preferred explanation was that the low rates reflected an absence of shallow magma (Stoiber et al., 1980, 1981; Casadevall et al., 1981, 1983). This inference was motivated by a temporary interruption, around 4–6 June 1980, of a pattern of inflation detected by just one tiltmeter 6 km southwest of the summit at Ape Cave North (Dvorak et al., 1981). Since increased $SO_{2(g)}$ emissions were sustained only after this time, it was assumed that the halt in inflation reflected completed emplacement of $\sim$2–5 km^3 of magma to shallow levels and that a prior absence of shallow magma explained the low rates before this time (Stoiber et al., 1980, 1981; Casadevall et al., 1981, 1983). This hypothesis has been called into question, however, since there was no evidence for edifice-wide deformation and intrusion-related seismicity as would be expected from emplacement of so large a quantity of magma to shallow depth (Pallister et al., 1992; J. Dvorak, pers. commun., 1995).

The surprisingly small noneruptive $SO_{2(g)}$ emissions from 29 March to 6 June, despite the paroxysmal eruption on 18 May, suggest that scrubbing may have been a factor in the early stages of degassing. Unfortunately, $CO_{2(g)}$ emission rate data are not available for comparison during this period. Several observations are nevertheless consistent with this interpretation. Water sampled by David Johnston on 23 April from the 15-m diameter pond ($T = 17$°C; pH = 5.97) at the bottom of a small newly created crater at Mount St. Helens was enriched in $Cl^-_{(aq)}$ (97 mg/l) and $SO^{2-}_{4(aq)}$ (36 mg/l) compared to local snowmelt (Barnes et al., 1981). Gas escaped in large amounts through the pond, and there was a strong $H_2S_{(g)}$ odor in the crater (observations by David Johnston reported in Barnes et al., 1981). It is also noteworthy that COSPEC investigators drew attention to the $H_2S_{(g)}$ odor in the vicinity of plumes prior to the 18 May eruption at times when noneruptive $SO_{2(g)}$ emissions rarely exceeded 10 t/d (Stoiber et al., 1980). Sulfur gas measurements made directly in plumes showed that $H_2S_{(g)}$ generally exceeded $SO_{2(g)}$ until after 4 June (Hobbs et al., 1981, 1982). Pale-blue flames were first observed in the summit crater on the night of 29 March and reported again in nighttime aerial observations through early April (Casadevall et al., 1981; Christiansen and Peterson, 1981). The chemistry of the flames was never positively identified, despite several attempts by David Johnston to do so, however it is well known that $H_2S_{(g)}$ burns in air with a pale-blue flame (The Merck Index, 1983). Since it was springtime, the ice-filled summit crater and several glaciers on the volcano flanks provided copious sources of water for the permeable edifice. Scientists who worked on the volcano at the time describe it as 'soaking wet' (C.D. Miller, pers. commun., 1995). Ample evidence exists for involvement of water in the pre-18 May phreatic eruptions as we summarize below from Christiansen and Peterson (1981). All these eruptions were steam-blasts and reflected the heating of the volcano by a small shallow intrusion that produced a conspicuously bulging north flank — the intrusion known subsequently as the 'cryptodome'. Ash from the phreatic eruptions was typically very wet and large amounts of water fell from the phreatic eruption columns. Small lakes formed, disappeared, and reformed within the summit area crater. The phreatic eruptions and ephemeral lakes strongly suggest a shallow hydrothermal system was present. After 22 April, fumaroles in the summit area crater continuously discharged white steam clouds, further indication of a boiling hydrothermal system. The rapidly bulging

north flank caused extreme fracturing of Forsyth Glacier between 27 March and 17 May. New steam vents appeared in the upper part of the bulge during the first half of May, and infrared scanning revealed numerous areas of thermal emission within the ice crevasses of that area. These observations indicate conditions favorable for melting and generation of water with ready access to the volcano via fractures forming in the rapidly inflating north flank. It is significant, in view of the low $SO_{2(g)}$ emissions, that later studies of the cryptodome dacite revealed abundant petrologic and stable isotope evidence of volatile loss from the intrusion after its shallow emplacement prior to the 18 May eruption (Hoblitt and Harmon, 1993). Hoblitt and Harmon (1993) attributed the apparent inconsistency between their results and the low $SO_{2(g)}$ emissions before 18 May to dissolution of the magmatic volatiles in a hydrothermal system, which they presumed surrounded the cryptodome.

The elevated $SO_{2(g)}$ emission rates after 6 June (Fig. 13b) imply that pathways from degassing magma to the atmosphere had become sufficiently dried out to prevent widespread scrubbing. We infer that drying of magmatic-gas pathways was caused mostly by intrusion within the conduit system coupled with boiling away of the hydrothermal system. The subsequent emplacement of a lava dome shortly thereafter following the 12 June eruption and the disappearance of a large lake (300–400 m × 50–75 m) within the crater after 11 June support this interpretation.

$SO_{2(g)}$ scrubbing was apparently active again during a period of unrest at Mount St. Helens in the summer of 1998. The number of well-located seismic events increased during May through mid-July as much as five-fold above the monthly rate of the previous winter. The earthquakes occurred chiefly in two clusters directly beneath the crater lava dome — one at 2–5 km below the dome, the other in the depth range 7–9 km. Very few earthquakes were shallower than 2 km. Airborne surveys in June and July indicated $CO_{2(g)}$ emission rates of 1500–2000 t/d, but in August and September $CO_{2(g)}$ emissions approached background levels (Gerlach et al., in preparation). COSPEC measurements made concurrently with the $CO_{2(g)}$ measurements were, however, unable to detect $SO_{2(g)}$ above background. The increase in seismicity and the release of $CO_{2(g)}$ were interpreted to reflect replenishment of the magma reservoir, whose top is ~7 km below the crater; the Cascades Volcano Observatory released information statements to this effect on 2 June and 1 July.

Dome fumaroles and crater hot springs were investigated during the summer of 1998 by R. Symonds. Fumarole samples obtained on 29 June from an 86°C vent on the September 1984 lobe on the dome, show that $CO_{2(g)}$ was the only detectable magmatic species in the gases and that both $CO_{2(g)}/SO_{2(g)}$ and $CO_{2(g)}/H_2S_{(g)}$ molar ratios exceed 9000; the site, the hottest fumarole on the dome since at least the mid-1980's, had actually cooled by 260–370°C since last sampled in 1994–1995 when the gases contained small amounts (<1%) of $H_2S_{(g)}$ and $HCl_{(g)}$ in addition to $CO_{2(g)}$ (R. Symonds, unpublished data). The odor of $H_2S_{(g)}$ was not apparent in the crater or in plume airborne surveys. Moreover, there was more snow and less steaming on the dome than during the 1994–1995 period.

On 6 August 1998, hot springs discharging between Loowit and Step canyons in northcentral part of the crater were investigated. The springs probably first surfaced in about 1996, although a crater debris flow in Fall 1997 covered some of the springs, which later resurfaced. Previous work has focused on hot springs in the Loowit and Step canyons (Shevenell and Goff, 1993), but the striking temperatures (up to 73°C) and spectacular, white travertine precipitates (up to several mm thick on downstream cobbles) in these new springs beckoned investigation. At the time of visit, these springs were neutral (pH = 6.5–6.9) and contained up to 790 mg/l $HCO^-_{3(aq)}$, 640 mg/l $Cl^-_{(aq)}$, 400 mg/l $SO^{2-}_{4(aq)}$, and 3.4 mg/l $F^-_{(aq)}$ (R. Symonds, M. Huebner, and R. Mariner, unpublished data). During the same crater investigation, the maximum temperature of the Source Hot Springs in the upper Loowit canyon (Shevenell and Goff, 1993) was 49°C, significantly cooler than the 64°C maximum measured by L. Mastin (pers. commun., 1998) in 1993–1994. The compositions of the crater springs are consistent with deep scrubbing of magmatic $HCl_{(g)}$, $CO_{2(g)}$, $SO_{2(g)}$, and $HF_{(g)}$ followed by wall–rock neutralization reactions en route to the surface, although some of the $Cl^-_{(aq)}$ and $SO^{2-}_{4(aq)}$ may also come from rock dissolution.

Owing to the large perceived amounts of dissolved magmatic volatiles in the Loowit and new crater springs, on 2 September R. Symonds and L. Mastin

measured the total discharge of $HCO^{-}_{3(aq)}$, $Cl^{-}_{(aq)}$, $SO^{2-}_{4(aq)}$, and $F^{-}_{(aq)}$ from crater springs and streams. The results suggest that significant amounts of magmatic gases (8.1 t/d of $HCl_{(g)}$, 6.2 t/d of $CO_{2(g)}$, 4.3 t/d of $SO_{2(g)}$, and 0.06 t/d HF) are scrubbed and discharged from the hydrothermal system (R. Symonds, L. Mastin, M. Huebner, and R. Mariner, unpublished data), assuming that scrubbing is the dominant source of these constituents in the springs. While these scrubbing estimates are lower than expected from the transient 1500–2000 t/d of $CO_{2(g)}$ discharged in June and July, note that: (1) the rates of spring discharge were measured in September when $CO_{2(g)}$ emissions approached background levels; and (2) additional discharge may occur through the groundwater system.

The airborne and ground-based findings are consistent with the inferred degassing of the intrusion and concomitant scrubbing of magmatic gases at a low g/w ratio; removal of $H_2S_{(g)}$ by reaction with ferrous iron may also have been involved. Prolonged melting of snow from the progressively growing permanent snowfield in the crater (Anderson et al., 1998), assured a wet edifice and favored a low g/w ratio. The results also point to expansion of the hydrothermal system as the subvolcanic system becomes progressively saturated with water.

3.3. Pinatubo

COSPEC measurements of $SO_{2(g)}$ emissions contributed importantly to the successful forecasting of the paroxysmal eruptions of Mount Pinatubo on 12, 13, and 15 June 1991 (Daag et al., 1996). Thirteen measurements spread over 28 days showed high emission rates in the month preceding these explosions (Fig. 13c). The first measurement on 13 May gave a rate of 500 t/d, a clear sign of significant magma degassing and the availability of dry pathways. $SO_{2(g)}$ output increased 10-fold by late May. A trend of logarithmically increasing emission rates began with COSPEC results of 1–1.5 kt/d on 7–8 June and then climbed to 13 kt/d on 10 June. The trend continued with TOMS results indicating 600 kt/d on 12 June, increasing to 4,300 kt/d on 13 June, and finally culminating at 53,300 kt/d in the 15 June eruption (Fig. 13c). Three COSPEC measurements after the paroxysmal explosions suggest that high $SO_{2(g)}$ emissions of 1–5 kt/d continued for at least another two months (Fig. 13c).

COSPEC monitoring may have been successful largely because intruding magma boiled off the preexisting hydrothermal system, thus drying out Pinatubo's interior and preventing wholesale scrubbing of acid gases even during the earliest $SO_{2(g)}$ measurements. Deep exploration wells drilled in 1988–1990 for geothermal energy confirmed the presence of an acidic hydrothermal system under the northwest flank of the volcano (Delfin et al., 1992, 1996). On 2 April 1991, phreatic explosions issued from a 1.5 km-long line of vents along a northeast-trending fissure on the upper north flank of the volcano (Wolfe and Hoblitt, 1996). These explosions, which marked the beginning of eruptive activity at Mount Pinatubo, were interpreted by Wolfe and Hoblitt (1996) to be of hydrothermal origin. They probably initiated the drying out of the volcano's hydrothermal system by vaporization and expulsion to the atmosphere through open system boiling. After the explosions, a line of active vents across the volcano's upper north flank continued to emit steam, presumably from the hydrothermal system. Activity soon concentrated at three especially powerful fumaroles that remained vigorous the rest of April and May. Steam plumes rose commonly 300–800 m, at times reaching 1500–3000 m, and eventually hurled steam and ash to 8000 m (Sabit et al., 1996). People in the vicinity of the phreatic explosions reported smelling $H_2S_{(g)}$ (Daag et al., 1996). US Air Force personnel reported intense and persistent $H_2S_{(g)}$ odors in the week following the phreatic explosions at a communication facility located about 13 km north of the vents (T. Gerlach, phone log notes, 8 April 1991). These reports are consistent with the boiling of the hydrothermal system, with or without concomitant scrubbing of $SO_{2(g)}$ injections from intruding magma. Strong 'sulfur odor' was partly responsible for causing some residents of villages on the northwest, west, and southwest slopes of the volcano to evacuate voluntarily (Sabit et al., 1996). Although the species causing 'sulfur odor' was not positively identified, we speculate that it was $H_2S_{(g)}$ in the days immediately after the 2 April explosions, but the possibility of increasing involvement of $SO_{2(g)}$ as the volcano dried out can not be discounted. The 500 t/d emissions of $SO_{2(g)}$ on 13 May suggest the

establishment of dry pathways somewhat before this date. Scrubbing of $SO_{2(g)}$ degassed from magma after 13 May was apparently trivial. The apparent fast rate of drying out of the hydrothermal system (or gas-venting pathways) may have been in part fortuitous, however, since it took place at the end of the dry season and just prior to the onset of Typhoon Yunya (Oswalt et al., 1996). Another factor favoring efficient drying out could have been the low permeability of the hydrothermal system (Michels et al., 1991; Delfin et al., 1992), which may have inhibited its capacity to recharge boiled-off water fast enough to prevent or greatly diminish pre-eruption $SO_{2(g)}$ emissions. Low permeability was a major reason why the hydrothermal system was deemed unsatisfactory for geothermal energy development (Delfin et al., 1992).

3.4. Popocatépetl

Popocatépetl produced high $SO_{2(g)}$ emission rates (>1 kt/d) for about a year before the first ash eruption of nonjuvenile material on 21 December 1994, in its current cycle of renewed activity (Galindo et al., 1998; Delgado et al., 2001). These high rates of emission continued, averaging $\sim 2-3$ kt/d, for more than another year until magmatic eruptions commenced in March 1996. In fact, high $SO_{2(g)}$ emissions were the outstanding sign of unrest at the volcano for several years; in contrast, signs of unrest based on seismicity and deformation were minor to modest. Popocatépetl is thus an example where scrubbing is relatively insignificant and has not seriously masked precursory degassing signals, although scrubbing has been proposed as a possible factor contributing to some of the variations observed in $SO_{2(g)}$ output at certain times (Delgado et al., 2001). Popocatépetl is therefore at the opposite end of the scrubbing spectrum from Crater Peak. We assume this status may reflect the relatively drier climate than at Crater Peak or Mount St. Helens.

4. Conclusions

(1) Gas scrubbing poses a challenge to the correct interpretation of volcano-monitoring data based on compositions and emission rates of gases. The magnitude of the challenge depends on the relative importance of processes that can alter the gas output from a volcano. Although generalizations can be made about the factors that control scrubbing, their importance at specific volcanoes should be evaluated case by case. Scrubbing is potentially greatest during the precursory and early stages of an eruptive cycle. It tends to be more important for volcanoes in wet climates (like the US Pacific Northwest) and climates that foster permanent snow cover (like Alaska or Kamchatka). Scrubbing is likely to be enhanced by long periods of dormancy, but diminished by more continuous activity, which should help promote dry pathways through the volcano, even in wet climates. It also depends on the volcano's ground-water hydrology; systems with high permeability allow more water to interact with rising magmatic gas, but impermeable systems should dry out more rapidly. In addition, scrubbing has a greater impact on gases that make strong acids ($SO_{2(g)}$, $HCl_{(g)}$, $HF_{(g)}$) in water than those that make weaker acids ($CO_{2(g)}$, $H_2S_{(g)}$). Finally, a host of processes influence strongly the partitioning of magmatic volatiles between vapor and water and thus affect scrubbing. Important among these are: (1) the extent of rock/water interaction (e.g. the reduction of $HF_{(g)}$ and $H_2S_{(g)}$ emissions by reactions with rock-derived aluminum and iron, respectively); (2) the confining pressure (e.g. high-pressure solutions absorb more gas in the liquid-only region, and enhance $SO_{2(g)}$ and $HCl_{(g)}$ emissions within the liquid-plus-gas region); (3) the solution's pH (e.g. the modeling supports the conclusions of Rowe et al. (1992) that $HCl_{(g)}$ exsolves extensively from extremely acidic hydrothermal solutions); (4) the activities of the major anions (e.g. increasing the activities of $Cl^-_{(aq)}$ can enhance the exsolution of $HCl_{(g)}$ from acidic hydrothermal solutions); and (5) the composition and redox state of the magmatic gas (e.g. sulfur is generally less completely scrubbed from high-pressure magmatic gases with higher $H_2S_{(g)}/SO_{2(g)}$). Another potentially important process that we have not modeled is the difference between open- and closed-system boiling in a hydrothermal system being supplied with volatiles by magma degassing at depth.

(2) Recalling that our main intent is to understand the chemical reactions of magmatic gases along their ascent pathway, and thereby to determine which gases to monitor at various stages in a cycle of volcanic unrest, from early precursory stages to post-eruption,

we offer the following conceptual guide. Early on, groundwater will exist between the magma chamber or ascending intrusion and the surface. Depending on the rates of magma supply and heat transfer, the groundwater will retreat from magma, as adjacent rocks heat up, and return as the rocks cool down. The resulting cycle of monitorable gases is $CO_{2(g)}$ and $H_2S_{(g)}$ in precursory stages; $CO_{2(g)}$, $H_2S_{(g)}$, $SO_{2(g)}$, $HCl_{(g)}$, and $HF_{(g)}$ in eruptive and intense passive degassing stages; and $CO_{2(g)}$ and $H_2S_{(g)}$ again in the declining stages. Of course, in the final stages any remaining shallow magma probably will have exhausted its volatiles and little degassing of any species would occur.

We stress that a geochemical monitoring strategy for *early* detection of shallow magma degassing should be based on those species that are: (a) abundant magmatic volatiles; (b) least soluble in silicate melts; and (c) least sensitive to scrubbing. $CO_{2(g)}$ is clearly the prime candidate for early emission rate monitoring. However, intense and persistent early $H_2S_{(g)}$ emissions are easily detected by anyone and should be taken seriously, because they can signal boiling-off of a hydrothermal system by intruding magma, with or without concomitant conversion of scrubbed $SO_{2(g)}$ to $H_2S_{(g)}$. To track dry-out progress after the early stages of activity, both $CO_{2(g)}$ and $SO_{2(g)}$ (or $HCl_{(g)}$) emission rates should be monitored. Finally, the modeling suggests that monitoring the ratios of gases with different water solubilities might help follow the dry-out process; in particular, the ratios $H_2O_{(g)}/CO_{2(g)}$, $SO_{2(g)}/CO_{2(g)}$, $CO_{2(g)}/HCl_{(g)}$, $SO_{2(g)}/H_2S_{(g)}$, $H_2S_{(g)}/CO_{2(g)}$, and possibly $HCl_{(g)}/HF_{(g)}$ might be useful given the abundance of these species and the sensitivity of these ratios to dry-out progress. Owing to the different solubilities of $HCl_{(g)}$ and $SO_{2(g)}$ in shallow low-pH solutions, $HCl_{(g)}/SO_{2(g)}$ would be useful in monitoring the drying out of a shallow acidic hydrothermal system. However, this study demonstrates that ratio changes are produced by several mechanisms, so interpretation of ratio data requires a case-by-case evaluation.

The results presented here together with earlier modeling of the flash vaporization of hydrothermal fluids to superheated vapor (Gerlach et al., 1996) make it highly probable that magma degassing is the source of sustained $SO_{2(g)}$ emissions of >100 t/d. It appears unlikely that merely causing a long-lived hydrothermal system to boil will produce much if any $SO_{2(g)}$. We expect that such established systems would be near equilibrium with alteration minerals in their host rocks, and thus lack the requisite low pH for generating $SO_{2(g)}$, even though they may possess elevated temperatures and high sulfate concentrations. On the other hand, when magmatic gases are discharged into a higher pressure hydrothermal system at a rate that generates hydrogen ions much faster than they can be consumed by water–rock reactions, a transient condition of low pH, high temperature, and high sulfate concentration may evolve that promotes hydrothermal $SO_{2(g)}$ production. In this situation, $SO_{2(g)}$ emissions may arise contemporaneously from both boiling hydrothermal fluid and direct magma degassing. Making a distinction between the two sources of $SO_{2(g)}$ in such emissions may not be possible; from a volcanic-hazard perspective, it is unimportant, since in either case, magma degassing is the immediate source of the $SO_{2(g)}$. Therefore, the emergence of $SO_{2(g)}$ emissions (>100 t/d) from a system previously degassing mostly $CO_{2(g)}$ and $H_2S_{(g)}$ should be recognized as a critical milestone in the cycle of volcanic unrest. Lower $SO_{2(g)}$ emissions may have sources unrelated to concomitant magma degassing, but they may also arise from incomplete scrubbing of magmatic $SO_{2(g)}$ injected into hydrothermal systems under dynamic conditions involving flash boiling; this may be especially likely when $SO_{2(g)}$ emissions are low and erratic.

(3) Scrubbing of acid volatiles released from magma supplied to subvolcanic magma chambers may go on for hundreds or thousands of years. Over time, this process will acidify groundwater which will dissolve and intensely alter competent volcanic rock, thereby increasing the susceptibility to landslides by weakening the overall edifice and producing instability along faults and other structures. Clay-size minerals in the alteration can also increase the potential reach of any consequent debris flows. Sufficient alteration to generate volcanic landslides can apparently be produced over a few thousand years.

Acknowledgements

Funding for this project came from the US

Geological Survey's Volcano Hazards Program and Global Change and Climate History Program. Earlier versions of this manuscript benefited from reviews by Patrick Allard, Terry Keith, Jake Lowenstern, Willie Scott, and Hiroshi Shinohara. We thank M. Huebner, L. Mastin, and R. Mariner for their help with studies on the Mount St. Helens hot springs.

Impetus for the modeling in this study came in part from an intense desire of the senior author to understand the origins of low-temperature (<160°C) fumarolic discharges from North American volcanoes like Mounts Baker and Mageik. Werner Giggenbach radiated that same burning desire to understand gases from bubbling pools and fumaroles from volcanic and geothermal systems around the world. We praise Werner for developing outstanding methods for collecting, analyzing and interpreting volcanic and geothermal fluids, and for his many insightful publications. But most of all, we thank him for inspirational and entertaining talks about White Island and Ruapehu; Werner understood well that science is done by people — not machines — and that roaring fumaroles, boiling lakes of acid, and sulfurous fume provide the real energy for gas geochemists.

References

Akaku, K., Reed, M.H., Yagi, M., Kai, K., Yasuda, Y., 1991. Chemical and physical processes occurring in the Fushime geothermal system, Kyushu, Japan. Geochem. J. 25, 315–334.

Anderson Jr., C.H., Behrens, C.J., Floyd, G.A., Vining, M.R., 1998. Crater firn of Mount St. Helens, Washington. J. Cave Karst Stud. 60, 44–50.

Armannsson, H., Gislason, G., Hauksson, T., 1982. Magmatic gases in well fluids aid the mapping of the flow pattern in a geothermal system. Geochim. Cosmochim. Acta 46, 167–177.

Barin, I., Knacke, O., 1973. Thermochemical Properties of Inorganic Substances. Springer, Berlin, 921pp.

Barnes, I., Johnston, D.A., Evans, W.C., Presser, T.S., Mariner, R.H., White, L.D., 1981. Properties of gases and waters of deep origin near Mount St. Helens. In: Lipman, P.W., Mullineaux, D.R. (Eds.), The 1980 Eruptions of Mount St. Helens, Washington. U.S. Geol. Surv. Prof. Pap. 1250, 233–237.

Bluth, G.J.S., Courtney, J.S., Sprod, I.E., Schnetzler, C.C., Krueger, A.J., Walter, L.S., 1995. Explosive emissions of sulfur dioxide from the 1992 Crater Peak eruptions, Mount Spurr Volcano, Alaska. In: Keith, T.E.C. (Ed.), The 1992 Eruptions of Crater Peak Vent, Mount Spurr Volcano, Alaska. U.S. Geol. Surv. Bull. 2139, 37–45.

Bluth, G.J.S., Doiron, S.D., Schnetzler, C.C., Krueger, A.J., Walter, L.S., 1992. Global tracking of the SO_2 clouds from the June, 1991 Mount Pinatubo eruptions. Geophys. Res. Lett. 19, 151–154.

Brantley, S.L., Borgia, A., Rowe, G., Fernandez, J.F., Reynolds, J.R., 1987. Poás volcano crater lake acts as a condenser for acid metal-rich brine. Nature 330, 470–472.

Brimhall, G.H., Ghiorso, M.S., 1983. Origin and ore-forming consequences of the advanced argillic alteration process in hypogene environments by magmatic gas contamination of meteoric fluids. Econ. Geol. 78, 73–90.

Burnham, C.W., 1979. Magmas and hydrothermal fluids. In: Barnes, H.L. (Ed.), Geochemistry of Hydrothermal Ore Deposits. 2nd ed. Wiley, New York, pp. 71–136.

Campita, N.R., Daag, A.S., Newhall, C.G., Rowe, G.L., Solidum, R.U., 1996. Evolution of a small crater lake at Mount Pinatubo. In: Newhall, C.G., Pungongbayan, R.S., (Eds.), Fire and Mud: Eruptions and Lahars of Mount Pinatubo, Philippines. Philippine Institute of Volcanology and Seismology, Quezon City and University of Washington Press, Seattle, pp. 435–442.

Casadevall, T.J., Johnston, D.A., Harris, D.M., Rose, W.I., Malinconico, L.L., Stoiber, R.E., Bornhorst, T.J., Williams, S.N., Woodruff, L., 1981. SO_2 emission rates at Mount St. Helens from March 29 through December, 1980. In: Lipman, P.W., Mullineaux, D.R. (Eds.), The 1980 eruptions of Mount St. Helens, Washington. U.S. Geol. Surv. Prof. Pap. 1250, 193–200.

Casadevall, T.J., Rose, W.I., Gerlach, T.M., Greenland, L.P., Ewert, J., Wunderman, R., Symonds, R., 1983. Gas emissions and the eruptions of Mount St. Helens through 1982. Science 221, 1383–1385.

Casadevall, T.J., de la Cruz-Reyna, S., Rose, W.I., Bagley, S., Finnegan, D.L., Zollar, W.H., 1984. Crater lake and post-eruption hydrothermal activity, El Chichón volcano, Mexico. J. Volcanol. Geotherm. Res. 23, 169–191.

Casadevall, T.J., Doukas, M.P., Neal, C.A., McGimsey, R.G., Gardner, C.A., 1994. Emission rates of sulfur dioxide and carbon dioxide from Redoubt Volcano, Alaska during the 1989–1990 eruptions. In: Miller, T.P., Chouet, B.A. (Eds.), The 1989–1990 eruptions of Redoubt Volcano, Alaska. J. Volcanol. Geotherm. Res. 62, 519–530.

Chase Jr., M.W., Curnutt, J.L., Downey Jr., J.R., McDonald, R.A., Syverud, A.N., Valenzuela, E.A., 1982. JANAF thermochemical tables, 1982 supplement. J. Phys. Chem. Ref. Data 11, 695–940.

Chase, M.W., Curnutt, J.L., Hu, A.T., Prophet, H., Syverud, A.N., Walker, L.C., 1974. JANAF thermochemical tables, 1974 supplement. J. Phys. Chem. Ref. Data 3, 311–480.

Chase, M.W., Curnutt, J.L., Prophet, H., McDonald, R.A., Syverud, A.N., 1975. JANAF thermochemical tables, 1975 supplement. J. Phys. Chem. Ref. Data 4, 1–175.

Christenson, B.W., 2000. Geochemistry of fluids associated with the1995–1996 eruptions of Mt. Ruahehu, New Zealand: signatures and processes in the magmatic-hydrothermal system. J. Volcanol. Geotherm. Res. 97, 1–30.

Christenson, B.W., Wood, C.P., 1993. Evolution of a vent-hosted hydrothermal system beneath Ruapehu Crater Lake, New Zealand. Bull. Volcanol. 55, 547–565.

Christiansen, R.L., Peterson, D.W., 1981. Chronology of the 1980 eruptive activity. In: Lipman, P.W., Mullineaux, D.R. (Eds.),

The 1980 Eruptions of Mount St. Helens, Washington. U.S. Geol. Surv. Prof. Pap., 1250, 17–30.

Crowley, J.K., Zimbelman, D.R., 1997. Mapping hydrothermally altered rocks on Mount Rainier, Washington, with Airborne Visible/Infrared Imaging Spectrometer (AVIRIS) data. Geology 25, 559–562.

Daag, A.S., Tubianosa, B.S., Newhall, C.G., Tuñgol, N.M., Javier, D., Dolan, M.T., Delos Reyes, P.J., Arboleda, R.A., Martinez, M.M.L., Regalado, M.T.M., 1996. Monitoring sulfur dioxide emissions at Mount Pinatubo. In: Newhall, C.G., Pungongbayan, R.S. (Eds.), Fire and Mud: Eruptions and Lahars of Mount Pinatubo, Philippines. Philippine Institute of Volcanology and Seismology, Quezon City and University of Washington Press, Seattle, pp. 409–414.

Delfin, F.G., Sussman, D., Ruaya, J.R., Reyes, A.G., 1992. Hazard assessment of the Pinatubo volcanic-geothermal system: Clues prior to the 15 June 1991 eruption. Trans. Geotherm. Res. Council 16, 519–528.

Delfin, F.G., Villarosa, H.G., Layugan, D.B., Clemente, V.C., Candelaria, M.R, Ruaya, J.R., 1996. Geothermal exploration of the pre-1991 Mount Pinatubo hydrothermal system. In: Newhall, C.G., Pungongbayan, R.S. (Eds.), Fire and Mud: Eruptions and Lahars of Mount Pinatubo, Philippines. Philippine Institute of Volcanology and Seismology, Quezon City and University of Washington Press, Seattle, pp. 197–212.

Delgado, G.H., Cardenas, G.L., Piedad, S.N., 2001. Sulfur dioxide emissions from Popocatépetl Volcano (Mexico): Case study of high-flux passively degassing erupting volcano. J. Volcanol. Geotherm. Res. 108, 107–120.

Doukas, M.P., Gerlach, T.M., 1995. Sulfur dioxide scrubbing during the 1992 eruptions of Crater Peak, Mount Spurr Volcano, Alaska. In: Keith, T.E.C. (Ed.), The 1992 Eruptions of Crater Peak Vent, Mount Spurr Volcano, Alaska. U.S. Geol. Surv. Bull. 2139, 47–57.

Drummond, S.E., Ohmoto, H., 1985. Chemical evolution and mineral deposition in boiling hydrothermal systems. Econ. Geol. 80, 126–147.

Dvorak, J., Okamura, A.T., Mortensen, C., Johnston, M.J.S., 1981. Summary of electronic tilt studies at Mount St. Helens. In: Lipman, P.W., Mullineaux, D.R. (Eds.), The 1980 Eruptions of Mount St. Helens, Washington. U.S. Geol. Surv. Prof. Pap. 1250, 169–174.

Eichelberger, J.C., Keith, T.E.C., Miller, T.P., Nye, C.J., 1995. The 1992 eruption of Crater Peak Vent, Mount Spurr Volcano, Alaska: Chronology and summary. In: Keith, T.E.C. (Ed.), The 1992 Eruptions of Crater Peak Vent, Mount Spurr Volcano, Alaska. U.S. Geol. Surv. Bull. 2139, 1–18.

Ellis, A.J., Mahon, W.A.J., 1977. Chemistry and Geothermal Systems. Academic Press, New York, 392 pp.

Farrar, C.D., Sorey, M.L., Evans, W.C., Howle, J.F., Kerr, B.D., Kennedy, B.M., King, C.Y., Southon, J.R., 1995. Forest-killing diffuse CO_2 emission at Mammoth Mountain as a sign of magmatic unrest. Nature 376, 675–677.

Galindo, I., Ivlev, L.S., Gonzalez, A., Ayala, R., 1998. Airborne measurements of particle and gas emissions from the December 1994–January 1995 eruption of Popocatépetl volcano (Mexico). J. Volcanol. Geotherm. Res. 83, 197–217.

Gardner, C.A., Neal, C.A., Waitt, R.B., Janda, R.J., 1994. Proximal pyroclastic deposits from the 1989–1990 eruption of Redoubt Volcano, Alaska — Stratigraphy, distribution, and physical characteristics. In: Miller, T.P., Chouet, B.A. (Eds.), The 1989–1990 Eruptions of Redoubt Volcano, Alaska. J. Volcanol. Geotherm. Res. 62, 213–250.

Gardner, C.A., Cashman, K.V., Neal, C.A., 1998. Tephra-fall deposits from the 1992 eruption of Crater Peak, Alaska: implications of clast textures for eruptive processes. Bull. Volcanol. 59, 537–555.

Gerlach, T.M., Casadevall, T.J., 1986. Fumarole emissions at Mount St. Helens Volcano, June 1980 to October 1981: degassing of a magma-hydrothermal system. J. Volcanol. Geotherm. Res. 28, 141–160.

Gerlach, T.M., McGee, K.A., 1994. Total sulfur dioxide emissions and pre-eruption vapor-saturated magma at Mount St. Helens, 1980–1988. Geophys. Res. Lett. 21, 2833–2836.

Gerlach, T.M., Westrich, H.R., Symonds, R.B., 1996. Preeruption vapor in magma of the climactic Mount Pinatubo eruption: Source of the giant stratospheric sulfur dioxide cloud. In: Newhall, C.G., Pungongbayan, R.S. (Eds.), Fire and Mud: Eruptions and Lahars of Mount Pinatubo, Philippines. Philippine Institute of Volcanology and Seismology, Quezon City and University of Washington Press, Seattle, pp. 415–433.

Giggenbach, W.F., 1980. Geothermal gas equilibria. Geochim. Cosmochim. Acta 44, 2021–2032.

Giggenbach, W.F., 1987. Redox processes governing in chemistry of fumarolic gas discharges from White Island. Appl. Geochem. 2, 143–161.

Giggenbach, W.F., 1988. Geothermal solute equilibria. Derivation of Na–K–Mg–Ca geoindicators. Geochim. Cosmochim. Acta 52, 2749–2765.

Giggenbach, W.F., García, P.N., Londoño, C.A., Rodriguez, V.L.A., Rojas, G.N., Calvache, V.M.L., 1990. The chemistry of fumarolic vapor and thermal-spring discharges from the Nevado del Ruiz volcanic-magmatic hydrothermal system, Columbia. J. Volcanol. Geotherm. Res. 42, 13–39.

Gill, J., 1981. Orogenic Andesites and Plate Tectonics. Springer, Berlin, 390pp.

Harris, D.M., Sato, M., Casadevall, T.J., Rose, W.I., Bornhorst, T.J., 1980. Emission rates of CO_2 from plume measurements. In: Lipman, P.W., Mullineaux, D.R. (Eds.), The 1980 Eruptions of Mount St. Helens, Washington. U.S. Geol. Surv. Prof. Pap. 1250, 201–207.

Hedenquist, J.W., Lowenstern, J.B., 1994. The role of magmas in the formation of hydrothermal ore deposits. Nature 370, 519–527.

Hemley, J.J., Jones, W.R., 1964. Chemical aspects of hydrothermal alteration with emphasis on hydrogen metasomatism. Econ. Geol. 59, 538–569.

Henley, R.W., Ellis, A.J., 1983. Geothermal systems ancient and modern: a geochemical review. Earth-Sci. Rev. 19, 1–50.

Hobbs, P.V., Radke, L.F., Eltgroth, M.W., Hegg, D.A., 1981. Airborne studies of the emissions from the volcanic eruptions of Mount St. Helens. Science 211, 816–818.

Hobbs, P.V., Tuell, J.P., Hegg, D.A., Radke, L.F., Eltgroth, M.W.,

1982. Particles and gases in the emissions from the 1980–1981 volcanic eruptions of Mt. St. Helens. J. Geophys. Res. 87, 11,062–11,086.

Hoblitt, R.P., Harmon, R.S., 1993. Bimodal density distribution of cryptodome dacite from the 1980 eruption of Mount St. Helens, Washington. Bull. Volcanol. 55, 421–437.

Holland, H.D., 1965. Some applications of thermochemical data to problems of ore deposits II. Mineral assemblages and the composition of ore-forming fluids. Econ. Geol. 60, 1101–1166.

Johnson, J.W., Oelkers, E.H., Helgeson, H.C., 1992. SUPCRT92: a software package for calculating the standard molal thermodynamic properties of minerals, gases, aqueous species, and reactions from 1 to 5000 bar and 0 to 1000°C. Comp. Geosci. 18, 899–947.

Keith, T.E.C. (Ed.), 1995. The 1992 eruptions of Crater Peak Vent, Mount Spurr Volcano, Alaska. U.S. Geol. Surv. Bull. 2139, 220 pp.

Keith, T.E.C., Thompson, J.M., McGimsey, R.G., 1995. Chemistry of crater lake waters prior to the 1992 eruptions of Crater Peak, Mount Spurr Volcano, Alaska. In: Keith, T.E.C. (Ed.), The 1992 Eruptions of Crater Peak Vent, Mount Spurr Volcano, Alaska. U.S. Geol. Surv. Bull. 2139, 59–63.

Kiyosu, Y., Kurahashi, M., 1983. Origin of sulfur species in acid-sulfate-chloride thermal waters, northeastern Japan. Geochim. Cosmochim. Acta 47, 1237–1245.

Le Guern, F., Gerlach, T.M., Nohl, A., 1982. Field gas chromatograph analyses of gases from a glowing dome at Merapi volcano, Java, Indonesia, 1977, 1978, 1979. J. Volcanol. Geotherm. Res. 47, 223–245.

López, D.L., Williams, S.N., 1993. Catastrophic volcanic collapse: relation to hydrothermal processes. Science 260, 1794–1796.

Matsuo, S., Suzuki, M., Mizutani, Y., 1978. Nitrogen to argon ratio in volcanic gases. In: Alexander Jr., E.C., Ozima, M. (Eds.), Terrestrial Rare Gases. Central Academic Publishing in Japan, Tokyo, pp. 17–25.

McGee, K.A., Casadevall, T.J., 1994. A Compilation of Sulfur Dioxide and Carbon Dioxide Emission-Rate Data from Mount St. Helens during 1980–1988. U.S. Geol. Surv. Open-File Rep. 94-212, 24 pp.

McGee, K.A., Gerlach, T.M., 1998. Annual cycle of magmatic CO_2 in a tree-kill soil at Mammoth Mountain, California: implications for soil acidification. Geology 26, 463–466.

Michels, D.E., Clemente, V.C., Ramos, M.N., 1991. Hydrochemical features of a geothermal test well in a volcanic caldera, Mt. Pinatubo, Philippines. Proceedings, Sixteenth Workshop on Geothermal Reservoir Engineering, Stanford University, Stanford, CA, 23–25 January, pp. 261–266.

Miller, T.P., 1994. Dome growth and destruction during the 1989–1990 eruption of Redoubt Volcano. In: Miller, T.P., Chouet, B.A. (Eds.), The 1989–1990 Eruptions of Redoubt Volcano, Alaska. J. Volcanol. Geotherm. Res. 62, 197–212.

Motyka, R.J., Nye, C.J., 1993. Fumarolic gas chemistry (1982) and thermal spring water chemistry, Crater Peak (1985), Mount Spurr, Alaska. In: Solie, D.N., Tannian, F. (Eds.), Short Notes on Alaskan Geology 1993. Alaska Department of Natural Resources, Division of Geological and Geophysical Surveys Professional Report, vol. 113, pp. 31–40.

Oswalt, J.S., Nichols, W., O'Hara, J.F., 1996. Meteorological observations of the 1991 Mount Pinatubo eruption. In: Newhall, C.G., Pungongbayan, R.S. (Eds.), Fire and Mud: Eruptions and Lahars of Mount Pinatubo, Philippines. Philippine Institute of Volcanology and Seismology, Quezon City and University of Washington Press, Seattle, pp. 625–636.

Pallister, J.S., Hoblitt, R.P., Crandell, D.R., Mullineaux, D.R., 1992. Mount St. Helens a decade after the 1980 eruptions: magmatic models, chemical cycles, and a revised hazards assessment. Bull. Volcanol. 54, 126–146.

Pankratz, L.B., 1982. Thermodynamic Properties of Elements and Oxides. US Bur. Mines Bull. 672, 509 pp.

Pankratz, L.B., 1984. Thermodynamic Properties of Halides. US Bur. Mines Bull. 674, 826 pp.

Pankratz, L.B., Mah, A.D., Watson, S.W., 1987. Thermodynamic Properties of Sulfides. US Bur. Mines Bull. 689, 427 pp.

Pankratz, L.B., Stuve, J.M., Gokcen, N.A., 1984. Thermodynamic Data for Mineral Technology. US Bur. Mines Bull. 677, 355 pp.

Pasternack, G.B., Varekamp, J.C., 1994. The geochemistry of the Keli Mutu crater lakes, Flores, Indonesia. Geochem. J. 28, 243–262.

Reed, M.H., 1982. Calculation of multicomponent chemical equilibria and reaction processes in systems involving minerals, gases and an aqueous phase. Geochim. Cosmochim. Acta 46, 513–528.

Reed, M.H., 1992. Origin of diverse hydrothermal fluids by reaction of magmatic volatiles with wall rock. In: Magmatic Contributions to Hydrothermal Systems and The Behavior of Volatiles in Magma. Geological Survey of Japan Report No. 279, pp. 135–140.

Reed, M.H., 1997. Hydrothermal alteration and its relationship to ore fluid composition. In: Barnes, H.L. (Ed.), Geochemistry of Hydrothermal Ore Deposits, 3rd ed. Wiley, New York, pp. 303–366.

Reed, M.H., 1998. Calculation of simultaneous chemical equilibria in aqueous–mineral–gas systems and its application to modeling hydrothermal processes. In: Richards, J., Larson, P. (Eds.), Techniques in Hydrothermal Ore Deposits Geology. Rev. Econ. Geol. 10, 109–124.

Reed, M.H., Spycher, N.F., 1984. Calculation of high temperature pH and mineral equilibria in hydrothermal waters, with application to geothermometry and studies of boiling and dilution. Geochim. Cosmochim. Acta 48, 1479–1492.

Reed, M.H., Spycher, N.F., 1985. Boiling, cooling, and oxidation in epithermal systems: a numerical modeling approach. Rev. Econ. Geol. 2, 249–272.

Reyes, A.G., 1990. Petrology of Philippine geothermal systems and the application of alteration mineralogy to their assessment. J. Volcanol. Geotherm. Res. 43, 279–309.

Reyes, A.G., 1991. Mineralogy, distribution and origin of acid alteration in Philippine geothermal systems. In: High-Temperature Acid Fluids and Associated Alteration and Mineralization. Geological Survey of Japan Report No. 277, pp. 59–65.

Rowe, G.L., 1994. Oxygen, hydrogen, and sulfur isotope systematics of the crater lake system of Poás Volcano, Costa Rica. Geochem. J. 28, 263–287.

Rowe, G.L., Ohsawa, S., Takano, B., Brantley, S.L., Fernandez,

J.F., Barquero, J., 1992. Using crater lake chemistry to predict volcanic activity at Poás Volcano, Costa Rica. Bull. Volcanol. 54, 494–503.

Rye, R.O., 1993. The evolution of magmatic fluids in the epithermal environment: The stable isotope perspective. Econ. Geol. 88, 733–753.

Rye, R.O., Bethke, P.M., Wasserman, M.D., 1992. The stable isotope geochemistry of acid sulfate alteration. Econ. Geol. 87, 225–262.

Sabit, J.P., Pigtain, R.C., de la Cruz, E.G., 1996. The west-side story: observations of the 1991 Mount Pinatubo eruptions from the west. In: Newhall, C.G., Pungongbayan, R.S. (Eds.), Fire and Mud: Eruptions and Lahars of Mount Pinatubo, Philippines. Philippine Institute of Volcanology and Seismology, Quezon City and University of Washington Press, Seattle, pp. 445–455.

Scott, K.M., Pringle, P.T., Vallance, J.W., 1995. Sedimentology, behavior, and hazards of debris flows at Mount Rainier, Washington. U.S. Geol. Surv. Prof. Pap. 1547, 56.

Scott, W.E., McGimsey, R.G., 1994. Character, mass distribution, and origin of tephra-fall deposits of the 1989–1990 eruption of Redoubt Volcano, south-central Alaska. In: Miller, T.P., Chouet, B.A. (Eds.), The 1989–1990 Eruptions of Redoubt Volcano, Alaska. J. Volcanol. Geotherm. Res. 62, 251–272.

Sedwick, P.N., McMurtry, G.M., Macdougall, J.D., 1992. Chemistry of hydrothermal solutions from Oele's Vents, Loihi Seamount, Hawaii. Geochim. Cosmochim. Acta 56, 3643–3667.

Shevenell, L., Goff, F., 1993. Addition of magmatic volatiles into the hot spring waters of Loowit Canyon, Mount St. Helens, Washington, USA. Bull. Volcanol. 55, 489–503.

Spycher, N.A., Reed, M.H., 1988. Fugacity coefficients of H_2CO_2, CH_4, H_2O and of H_2O–CO_2–CH_4 mixtures: a virial equation treatment for moderate pressures and temperatures applicable to calculations of hydrothermal boiling. Geochim. Cosmochim. Acta 52, 739–749.

Spycher, N.F., Reed, M.H., 1989. Evolution of a Broadlands-type epithermal ore fluid along alternative P–T paths: implications for the transport and deposition of base, precious, and volatile metals. Econ. Geol. 84, 328–359.

Stoiber, R.E., Rose Jr., W.I., 1970. The geochemistry of Central American volcanic gas condensates. Geol. Soc. Am. Bull. 81, 2891–2912.

Stoiber, R.E., Williams, S.N., Malinconico, L.L., 1980. Mount St. Helens, Washington, 1980 volcanic eruption: magmatic gas component during first 16 days. Science 208, 1258–1259.

Stoiber, R.E., Williams, S.N., Malinconico, L.L., Johnston, D.A., Casadevall, T.J., 1981. Mt. St. Helens: Evidence of increased magmatic gas component. J. Volcanol. Geotherm. Res. 11, 203–212.

Stull, D.R., Prophet, H., 1971. JANAF thermochemical tables, 2nd ed. National Bureau of Standards Reference Data Series NBS-37, 1141 pp.

Sturchio, N.C., Williams, S.N., Garcia, P.N., Londoño, C.A., 1988. The hydrothermal system of Nevado del Ruiz Volcano, Columbia. Bull. Volcanol. 50, 399–412.

Symonds, R.B., Reed, M.H., 1993. Calculation of multicomponent chemical equilibria in gas–solid–liquid systems: calculation methods, thermochemical data and applications to studies of high-temperature volcanic gases with examples from Mount St. Helens. Am. J. Sci. 293, 758–864.

Symonds, R.B., Rose, W.I., Bluth, G.J.S., Gerlach, T.M., 1994. Volcanic-gas studies: methods, results, and applications. In: Carrol, M.R., Holloway, J.R. (Eds.), Volatiles in Magmas. Rev. Mineral. 30, 1–66.

Symonds, R.B., Janik, C.J., Evans, W.C., Ritchie, B.E., Counce, D., Poreda, R.J., Iven, M., 2001. Scrubbing masks magmatic degassing during repose at Cascade-Range and Aleutian-Arc Volcanoes. In preparation.

Takano, B., Watanuki, K., 1990. Monitoring of volcanic eruptions at Yugama crater lake by aqueous sulfur oxyanions. J. Volcanol. Geotherm. Res. 40, 71–87.

Takano, B., Ohsawa, S., Glover, R.B., 1994. Surveillance of Ruapehu Crater Lake, New Zealand, by aqueous polythionates. J. Volcanol. Geotherm. Res. 60, 29–57.

The Merck Index, 1983. An Encyclopedia of Chemistry and Drugs, 10th ed. Merck & Co., 2175 pp.

White, D.E., 1957. Thermal waters of volcanic origin. Geol. Soc. Am. Bull. 68, 1637–1658.

Williams, S.N., Calvache, V.M.L., López, D., Schaefer, S.J., 1992. Carbon dioxide emissions to the atmosphere by volcanoes. Geochim. Cosmochim. Acta 56, 1765–1770.

Williams, S.N., Sturchio, N.C., Calvache, V.M.L., Mendez, R.F., Londoño, C.A., Garcia, N.P., 1990. Sulfur dioxide from Nevado del Ruiz Volcano, Columbia: total flux and isotopic constraints on its origin. J. Volcanol. Geotherm. Res. 42, 53–68.

Wolfe, E.W., Hoblitt, R.P., 1996. Overview of the eruptions. In: Newhall, C.G., Pungongbayan, R.S. (Eds.), Fire and Mud: Eruptions and Lahars of Mount Pinatubo, Philippines. Philippine Institute of Volcanology and Seismology, Quezon City and University of Washington Press, Seattle, pp. 3–20.